
C2FAR: Coarse-to-Fine Autoregressive Networks for Precise Probabilistic Forecasting

Shane Bergsma Timothy Zeyl Javad Rahimipour Anaraki Lei Guo
Huawei Cloud, Alkaid Lab Canada
{shane.bergsma,timothy.zeyl,javad.anaraki,leiguo}@huawei.com

Abstract

We present coarse-to-fine autoregressive networks (C2FAR), a method for modeling the probability distribution of univariate, numeric random variables. C2FAR generates a hierarchical, coarse-to-fine discretization of a variable autoregressively; progressively finer intervals of support are generated from a sequence of binned distributions, where each distribution is conditioned on previously-generated coarser intervals. Unlike prior (flat) binned distributions, C2FAR can represent values with exponentially higher precision, for only a linear increase in complexity. We use C2FAR for probabilistic forecasting via a recurrent neural network, thus modeling time series autoregressively in both space and time. C2FAR is the first method to simultaneously handle discrete and continuous series of arbitrary scale and distribution shape. This flexibility enables a variety of time series use cases, including anomaly detection, interpolation, and compression. C2FAR achieves improvements over the state-of-the-art on several benchmark forecasting datasets.

1 Introduction

Probabilistic forecasting is the task of estimating a joint distribution over future values of a time series, given a sequence of historical values. As an important problem with many applications and an abundance of real-world data, probabilistic forecasting has unsurprisingly come to be dominated by deep learning methods [7]. Such methods typically fit a global sequence model to a dataset of related time series. To forecast a given series, future values are iteratively generated from one-step-ahead univariate output distributions. In this paper, we propose coarse-to-fine autoregressive networks (C2FAR), a general method for modeling distributions of univariate numeric data, and we show how C2FAR enables improved output distributions for probabilistic forecasting.

Such improvements are needed because time series offer challenges not present in applications like text and image modeling. First, dynamic range or *scale* of real-world time series can vary widely within a single dataset [57]. The typical solution is to normalize the data based on input historical values, but many time series have heavy tails [21], meaning even after normalization, future values must be modeled via distributions with unbounded support. Second, even within one dataset, time series may be discrete, continuous, or mixed, and each of these may be distributed in arbitrary, multi-modal ways, which vary over time. All of this makes it difficult for practitioners to encode input values and to select appropriate parametric forms for output distributions.

C2FAR allows efficient modeling of any univariate numeric output (§3). C2FAR extends prior work using categorical output distributions over binned representations [51, 21]. While the precision of prior methods is limited by the number of bins in the discretization, C2FAR achieves an exponential increase in precision through only a linear increase in the number of bin parameters. Like digits in the decimal number system (and unlike, say, roman numerals or simple tally marks), C2FAR represents scalar quantities hierarchically, treating numbers as multidimensional objects, with each successive dimension or *level* representing the original value at a progressively finer resolution (Fig. 1).

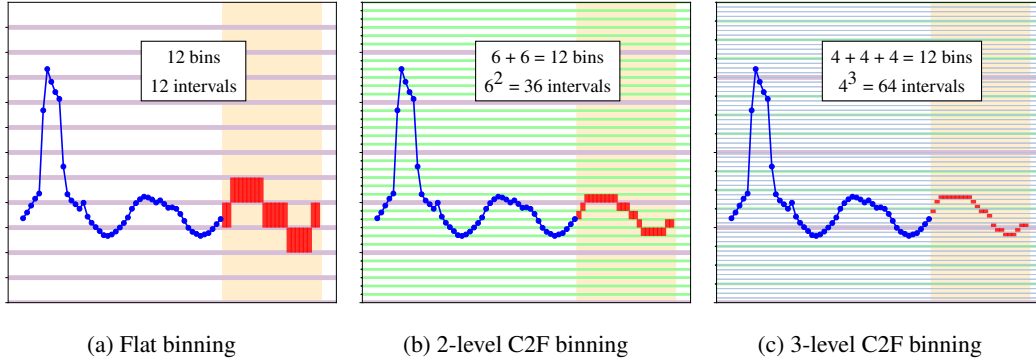


Figure 1: Flat vs. coarse-to-fine binnings for a *traff* time series (§5). C2F discretizations specify bin indices from coarse-to-fine, e.g. 3, 2, 2. For the same total number of bins, the number of unique intervals in a C2F binning is much higher (and thus reconstruction error is much lower).

C2FAR proposes an autoregressive generative model for such representations. Levels are generated hierarchically from coarse to fine. Finer and finer intervals of support are generated from a sequence of categorical (binned) distributions, each distribution conditioned on the previously-generated coarser intervals. The conditional distributions are parameterized by a neural network, and the model is fit by maximizing log-likelihood of observed data. Compared to flat binnings, C2FAR models are more efficient for a given level of precision, and better enable learning of order and distance.

We use C2FAR to model output distributions in a deep forecasting model based on DeepAR [57] (§4). In our experiments, C2FAR-based forecasting models better recover synthetic distributions compared to recent state-of-the-art methods (§5.1). Evaluation on benchmark forecasting datasets shows that, in contrast to prior work, discretization improves accuracy (§5.2). Multi-level C2FAR models further improve over flat binnings across all datasets, including evaluation on a large new dataset of public cloud demand, which we release as a paper supplement. Code and data for C2FAR are available at https://github.com/huaweicloud/c2far_forecasting.

2 Background and related work

2.1 Probabilistic neural forecasting, use of binned output distributions

Probabilistic forecasting architectures include LSTMs [74, 57], temporal convolutions [60, 15] and transformers [39, 80, 75]. While C2FAR can be used with any such architecture, for simplicity we restrict our discussion in this paper to models that are autoregressive in time [39, 57]. While non-AR models typically output best-guess point forecasts [12, 60, 80] or specific quantiles of interest [74, 22], they can be made to output C2FAR parameters at all horizons (as was done with Gaussians in [15]).

Autoregressive networks must define step-wise input and output. To handle series of very different *scales*, input values are often normalized (e.g., dividing values by their mean [39, 57, 51]); output values are scaled back after prediction. A density over outputs is achieved by mapping network states to location and spread parameters of specific distributions. Practitioners must choose a distribution “to match the statistical properties of the data” [57]. In practice, Gaussian [57, 39], Student’s-t [2], and Gaussian mixture distributions [48] have been used for real-valued data, while a negative binomial distribution [57] has been employed for discrete. Since output uncertainty is often not well captured by standard parametrics, recent work has investigated more flexible outputs, including spline quantile functions [26] and implicit quantile networks [30], which we compare to below (§5).

Rabanser et al. [51] use a categorical output distribution over a binned representation. Categoricals are flexible, but do not encode any underlying concept of bin order or distance (which must be learned). In prior work on pixel modeling, categorical distributions sometimes work better [72], sometimes worse [55] than mixture densities. In [51], the benefits of binning were mixed, and harmed DeepAR accuracy. Ehrlich et al. [21] “splice” a continuous Pareto distribution into a categorical in

order to model extreme values; we show how Pareto distributions can also be used when samples are generated autoregressively using C2FAR (§3).

2.2 Challenges in forecasting mixed data, the density spike issue

Many time series are either fully discrete (e.g., counts), or continuous but with “clumps” at particular values. Dollar values are often specified to two decimal places. Even intrinsically continuous series are always processed or serialized to a certain precision; for example, one version of *elec* has been quantized to integers, another to six decimal places (§5). As a cloud provider, we observe many *semicontinuous* [44] series, with significant probability of being either 0% or 100%, while otherwise being continuous (*zero-inflation* is also common in fully discrete demand data [14, 59]).

Modeling discrete data can be challenging. The inherent limits of discrete series are rarely known at prediction time, so unbounded distributions such as negative binomials must be used [63]. Unfortunately, it is “not possible” for such distributions to output values in a normalized domain [57], precluding valuable scale-normalization. But since real-valued forecasts are usually acceptable for discrete data, practitioners often simply normalize discrete data and train continuous models. Gouttes et al. [30] report better results on *wiki* with a Student’s-t distribution than with a negative binomial. Rabanser et al. [51] normalize *wiki* prior to “discretizing” it again for their categorical. We have also encountered practitioners with the (erroneous) belief that normalizing makes discrete data continuous.

Unfortunately, fitting powerful continuous models to discrete/mixed data “can lead to arbitrarily high density values, by locating a narrow high density spike on each of the possible discrete values” [71]. While this is a known issue in image modeling [69], it is apparently not well appreciated in forecasting. Density models based on splines [26] or flows [54] should therefore not be trained directly to maximize likelihood, as this may guide parameters (e.g., spline *knot* positions) solely to enable density spikes. A potential solution is *dequantizing*, e.g., adding `Uniform[0, 1]` noise as in [54]. But this assumes: (1) we know the discrete series a priori, and (2) the resulting loss in precision does not outweigh the benefits of continuous models. For C2FAR, the ability to locate high-density spikes on discrete values is a feature, not a bug. C2FAR does not generate *arbitrarily* narrow spikes, rather it is restricted by the precision of the hierarchical binning. C2FAR can therefore train for likelihood on the actual discrete data, and it can generate realistic samples reflecting the true data distribution.

2.3 Coarse-to-fine representations, hierarchical softmaxes

Coarse-to-fine binnings have been used previously in machine learning. A coarse-to-fine representation is induced by algorithms that recursively discretize continuous-valued attributes for decision tree classifiers [23]. On the output side, SSR-Net [77] classifies human age in a coarse-to-fine (but not autoregressive) manner. *i*SAX [61] uses a coarse-to-fine representation for indexing time series.

Prior autoregressive models of discrete data can be viewed as instances of C2FAR. WaveRNN [35] models 16-bit audio samples by generating first the coarse (high) 8-bits, then the fine (low) 8-bits, conditioned on the sampled coarse. Vipplerla et al. [73] found a different split between coarse and fine bits resulted in lower cross-entropy. These approaches can be regarded as two-level C2FAR models with classifier conditionals. The multi-stage likelihood from [59] can be viewed as a three-level C2FAR model, with binary classification at level 1 and 2, and Poisson regression to generate final counts. C2FAR unifies these approaches and generalizes them to unbounded, mixed/continuous data.

Beyond numeric data, hierarchical decompositions of categorical output distributions have been used previously in language modeling [47, 46]. As with C2FAR, the key benefit is exponentially fewer computations than when predicting words with a flat softmax. Whether further efficiencies such as variable-length representations (based on Huffman coding) [43] could prove effective when modeling continuous and ordinal data with C2FAR merits further investigation.

3 C2FAR networks

The process of discretization first partitions the support of a continuous variable into a finite number of distinct *bins*. A value is discretized by mapping it to the index of its corresponding bin. With C2FAR, partitioning is hierarchical: the support is first divided into a number of coarse bins, each of these coarse bins is further divided into a number of finer bins, and so on (recall Fig. 1 in §1). C2FAR

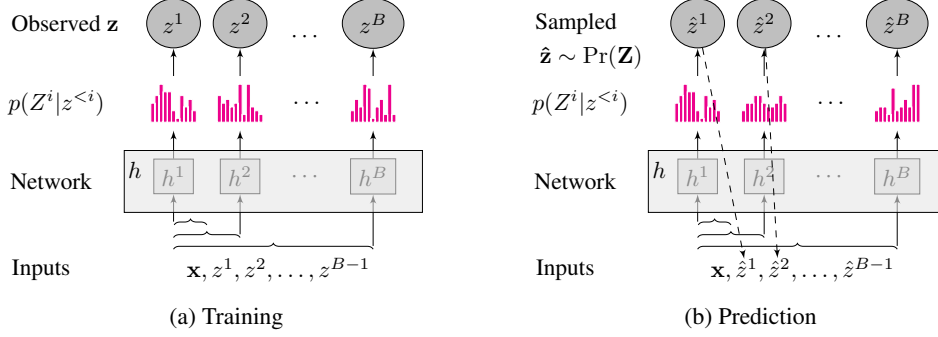


Figure 2: C2FAR network for regression. We train to minimize NLL of a set of examples; log loss on each example decomposes into the sum of NLL of each z^i under its categorical distribution. In prediction, we sample from the categoricals, and autoregressively use the sampled values as inputs.

thereby discretizes a data point, z , into a vector of B indices for each of the B coarse-to-fine levels, $\mathbf{z} = (z^1, \dots, z^B)$. More formally, C2FAR assumes a discretization function $d: \mathbb{R} \rightarrow (\mathcal{B}_1, \dots, \mathcal{B}_B)$, where each \mathcal{B}_i has one of $|\mathcal{B}_i|$ distinct values. Function d^{\leftarrow} is a kind of inverse of d , mapping a set of bin indices to an *interval* in the original real-valued domain, $d^{\leftarrow}: (\mathcal{B}_1, \dots, \mathcal{B}_B) \rightarrow (\mathbb{R}, \mathbb{R})$.

Let $\mathbf{z} = d(z)$ be the B -dimensional discretization of z . Let $\mathbf{z}^{<i}$ denote the first $i - 1$ bin indices, z^1, \dots, z^{i-1} . Let \mathbf{x} be an optional set of features that may inform z 's distribution (e.g., for mixed data, \mathbf{x} could flag which output bins contain integers). We follow prior work in modeling *multivariate* conditional distributions $p(\mathbf{z}|\mathbf{x})$ as autoregressive generative models via the chain rule [24, 6, 70]:

$$p(\mathbf{z}|\mathbf{x}) = \prod_{i=1}^B p(z^i|\mathbf{x}, \mathbf{z}^{<i}) \quad (1)$$

In C2FAR, each of the one-dimensional distributions, $p(z^i|\mathbf{x}, \mathbf{z}^{<i})$, is a categorical over the set of bin indices at the i th granularity, \mathcal{B}_i . Intuitively, the i th categorical is a distribution over the support *within* the generated $(i - 1)$ th bin. We parameterize these distributions using neural networks with a softmax output layer (specific architectures are discussed below), and fit the parameters to minimize negative log-likelihood (NLL) of training data (Fig. 2a). C2FAR is agnostic toward the encoding of the inputs z^i ; they may, for example, be represented with 1-hot-encodings or embedding layers. As a generative model, we synthesize new data by first sampling a coarse bin (\hat{z}^1) given \mathbf{x} , then iteratively sampling finer and finer bins given the sampled (and encoded) coarser values (Fig. 2b).

C2FAR supports a variety of neural architectures: following prior work in multivariate distribution modeling, we may use a separate (feedforward) network for each categorical [6] (as in Fig. 2), or one global network with masking to enforce the autoregressive property [28]. Separate networks may share parameters across the levels [38] or with classifications at the same level across time (§4). Having separate networks for each level means the modeling problem at a given level need not change if we add more levels to the hierarchy; we adopt this approach in our forecasting experiments (§4.2).

While not strictly required, we use linear (evenly-spaced) binnings at each level. We hypothesize this enables the finer networks to better generalize learned concepts of order and distance (i.e., regardless of the coarse bins that they are conditioned on). We refer to the span from the first interval to the last interval as the *extent* of the binning. The extent, the number of levels, and the number of bins at each level, are C2FAR hyperparameters. We also consider the extreme high/low intervals to be open-ended, terminating at $\pm\infty$; we discuss the implications of this below.

Level $B + 1$ parametric distributions. Let (a, b) be the interval defined by $(a, b) = d^{\leftarrow}(\mathbf{z})$. To complete our generative story, we must generate a value within (a, b) (rather than choosing a single “reconstruction value” for each bin as in [51]). Since our extreme intervals are open-ended, we cannot interpret our model as a piecewise uniform distribution [72], as uniforms are only defined on finite intervals. C2FAR solves this by allowing different distributions to be used depending on the interval (a, b) . Essentially, we assume a final conditional in (1) (implicitly at level $B + 1$) that generates from

a (differentiable) parametric distribution. We use distributions of the form:

$$p(Z^{B+1}|a, b) \sim \begin{cases} \text{Uniform}[a, b] & -\infty < a \text{ and } b < \infty \\ \text{Pareto}[a, \alpha_1] & b = \infty \\ -\text{Pareto}[b, \alpha_2] & a = -\infty \end{cases} \quad (2)$$

Here Pareto indicates a Type I Pareto distribution with fixed scale parameter (a or b , defined a priori from the extent of the binning in the observed space) and dynamic shape parameter α_i . Parameters α_1 and α_2 are generated by the h_{B+1} neural network in a manner analogous to how DeepAR outputs the mean and variance parameters of a Gaussian distribution [57].¹ We are effectively defining a piecewise-uniform density with Pareto-distributed tails.² We use this model for both continuous and discrete data. If data are truly discrete and precision is useful, our tuning procedure will choose more bins/levels. If one knows a priori the true discrete support, one may instead use discrete distributions at level $B + 1$, such as negative binomials, Poisson regression [59], or discrete uniforms.

Complexity. Consider a C2FAR discretization with B levels and an unvarying cardinality of K bins at each level; the original support of z is effectively partitioned into K^B total intervals, but modeled using only KB categorical outputs in total (B softmaxes with K values each). We may regard C2FAR as a K -ary tree of height B . At each node in the tree, we determine which of the K bins we fall into at that level, and follow the chosen branch to the sub-tree at the next level. We need only evaluate the softmax probabilities (and backpropagate gradients) for the B nodes on the path from the root to the leaf of the tree. Since the height of the tree, B , is logarithmic (in base K) over the total number of intervals, we compute exponentially fewer outputs with C2FAR compared to flat binnings. The final likelihood additionally requires computing the probability at the $B + 1$ level according to the corresponding parametric distribution (Uniform or Pareto) as given in Eqn. (2). In this way, full C2FAR densities are never explicitly manifested when training or predicting; for plotting (e.g., Fig. 6), we explicitly compute likelihood at tiny increments over a predefined range.

4 Forecasting with C2FAR

We now explain how C2FAR can be used for N -step-ahead probabilistic forecasting. We base the forecasting framework on DeepAR [57], which has served as the basis for other recent improvements in forecast distribution modeling [26, 30], and therefore facilitates experimental comparison (§5).

4.1 DeepAR-style probabilistic forecasting

Let z_t be the value of a time series at time t , and \mathbf{x}_t be a vector of time-varying features or *covariates*. Probabilistic forecasting aims to model the conditional distribution of N future values of z_t (the *prediction range*) given the $T + N$ covariates, and T historical values (the *conditioning range*):

$$p(z_{T+1} \dots z_{T+N} | z_1 \dots z_T, \mathbf{x}_1 \dots \mathbf{x}_{T+N}) \stackrel{\text{def}}{=} p(z_{T+1:T+N} | z_{1:T}, \mathbf{x}_{1:T+N}) \quad (3)$$

DeepAR [57] formulates this conditional distribution as an autoregressive generative model:

$$p(z_{T+1:T+N} | z_{1:T}, \mathbf{x}_{1:T+N}) = \prod_{t=T+1}^{T+N} p(z_t | z_{1:t-1}, \mathbf{x}_{1:T+N}) = \prod_{t=T+1}^{T+N} p(z_t | \theta_t = y(h_t))$$

where $h_t = \text{rnn}(h_{t-1}, z_{t-1}, x_t)$ is the output of an LSTM [32] recurrent neural network, and $y(\cdot)$ is a function that maps the output of the LSTM to the parameters of a parametric distribution $p(z_t | \theta_t)$. For example, $p(z_t | \theta_t)$ could be a Gaussian and $y(\cdot)$ output the Gaussian’s mean and variance as θ_t .

¹In this way, “weighted” Pareto tails are not “spliced” into the distribution at fixed user-defined quantiles, as they are in [21]. In C2FAR, Pareto tails provide the probability density function of values in the extreme bin, *given the values are in the extreme bin*. Each Pareto density itself integrates to 1, but is dynamically “weighted” by the probability of being in the corresponding extreme bin. Note also that if data does not have heavy tails, alternative distributions may be used in the extreme bins instead, e.g., left and right-truncated Gaussians.

²By parameterizing the quantile function with linear splines, SQF-RNN [26] actually enforces piecewise uniformity, over a *finite* range. Neural spline flows [20] require derivatives of the spline functions to match at knots, to avoid “numerical issues.” By parameterizing the PDF directly using classifiers, and only manifesting the portion needed, C2FAR has none of the above restrictions, while being more efficient and well-behaved.

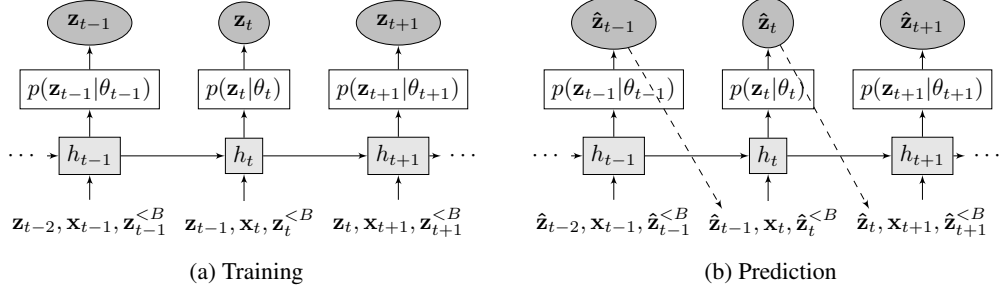


Figure 3: High-level C2FAR-RNN for forecasting. Unlike DeepAR, C2FAR-RNN uses discretized input/output vectors, \mathbf{z}_t , rather than scalars, and has additional (autoregressive) inputs $\mathbf{z}_t^{}$.

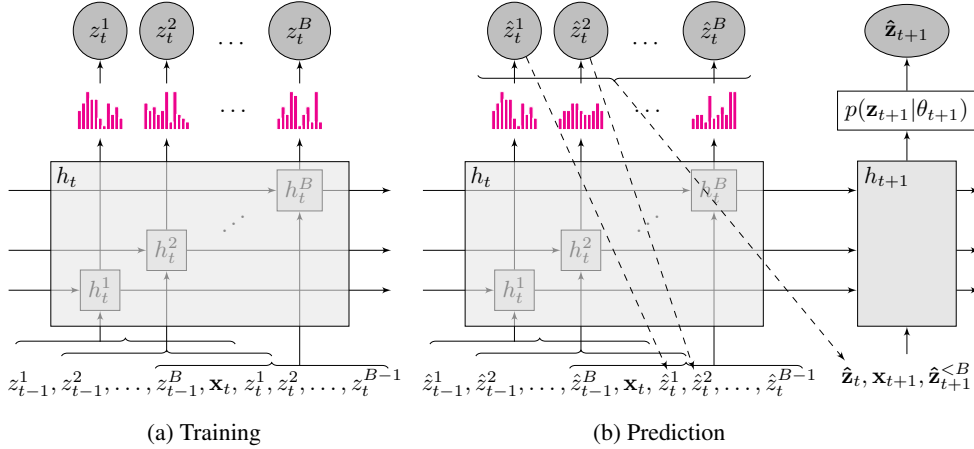


Figure 4: C2FAR-RNN model detailing high-level unit, h_t , from Fig. 3. We train to minimize sum of NLL at each z_t^i under a categorical with parameters given by a level-specific RNN, h_t^i . We predict by sequentially sampling a discretization at each time step, \mathbf{z}_t , which is re-input at step $t + 1$.

Fig. 3a illustrates the overall architecture (with additions for C2FAR noted). Information about the conditioning range $z_1 \dots z_T$ is conveyed through the state of the network at time T (i.e., h_T). From an encoder-decoder perspective [65, 3], DeepAR uses the same network to encode and decode.

For training, each series is sliced into multiple *windows*, i.e., conditioning+prediction ranges at different start points. Windows are normalized using their conditioning ranges, and parameters are fit to minimize NLL of prediction-range outputs. To generate a forecast for a given (normalized) conditioning range, DeepAR draws samples $\hat{z}_{T+1} \dots \hat{z}_{T+N}$ in sequence from $p(z_t | \theta_t)$ (Fig. 3b). Sampled roll-outs are unnormalized, and by repeating this procedure many times, a Monte Carlo estimate of (3) is obtained, from which desired forecast quantiles can be derived (see, e.g., Fig. 7).

4.2 Forecasting with C2FAR: C2FAR-RNN

We augment DeepAR by converting time series to their C2FAR discretization $\mathbf{z}_t = d(z_t)$. Rather than generating θ_t in one shot at each time step, we generate C2FAR categoricals autoregressively *within* each time step (Fig. 4). Each generated bin index, z_t^{i-1} , thus informs the distribution of the next bin index at that time step z_t^i . We also leverage information about discretized values at earlier time steps by replacing C2FAR’s classifier-based conditionals (§3, Fig. 2) with LSTMs, one for each level in the C2FAR hierarchy. Intuitively, when generating bin index z_t^i , our inputs comprise both our current position in higher-level bins (e.g. z_t^{i-1}) *and* the i th-level index at the previous time step (z_{t-1}^i), along with the previous LSTM state, h_{t-1}^i .

We call the resulting system C2FAR-RNN. As with DeepAR, C2FAR-RNN is trained to minimize NLL of observed outputs in (normalized) prediction ranges (Fig. 4a). During training (and when

evaluating NLL of test sequences), *at each time step*, all values are known and all distributions can be computed *in parallel*. When predicting (Fig. 4b), we must sample each bin index z_t^i *sequentially*.

Recall that C2FAR has an implicit $B + 1$ level, where a real value is generated from a parametric distribution (Eqn. (2)). We do not use an RNN for this level; the uniform distributions are fully-specified by the interval endpoints, while we generate Pareto parameters (α_1, α_2) via a simple feed-forward neural network (with a single hidden layer and softplus output transformation). To help inform the Pareto networks, we also encode real-valued z_{t-1} as an additional input/covariate.

Complexity. Let H be the number of RNN hidden units, K a constant number of bins per level, and B the number of levels ($I = K^B$ total intervals). The complexity-per-timestep of *each RNN* is essentially the sum of the RNN’s recurrence operation, $H \times H$, and the projection of the recurrence to output bins, $K \times H$. For flat binnings, *overall* complexity is typically dominated by $K \times H$, while B -level C2FAR-RNN models are dominated by $B \times H \times H$, i.e., the cost of running B RNNs in parallel. Measurements of timing and memory consumption (supplemental Table 9, 10) are well explained by these observations and corresponding values for H , K , and B (supplemental Table 7).³

Tuning. While C2FAR is trained for NLL, it is *tuned* for a given target metric. For forecasting, the metric is multi-step-ahead error. Thus we evaluate our forecasts during training by periodically running Monte Carlo sampling on our validation set and computing multi-step-ahead error. For tasks such as anomaly detection, denoising, etc., we would train for NLL and tune for an application-specific metric. While there is no one-size-fits-all metric for evaluating generative models, log-likelihood itself is sometimes regarded as the de facto standard [69]. Ironically, this is the one loss function C2FAR can *not* tune for, at least not on discrete data, because of the density spike issue (§2.2); if we tune directly for NLL, the tuner chooses more and more bins and levels, leading to narrower and higher spikes. If we *must* tune for log-likelihood, we could use discrete distributions in the $B + 1$ level. We could also add uniform noise, as other approaches do (but note in prior work this is required to enable *training*, not *tuning*, on discrete data). NLL evaluations are explored in supplemental §E.

4.3 Limitations and broader impact of C2FAR forecasting

Every B -level C2FAR model has an equally *expressive* [52] flat counterpart with a single categorical over all the fine-grained intervals; given unlimited training data, C2FAR may therefore not offer modeling benefits over flat binning. Conversely, when there is limited data, simple parametric distributions, with fewer parameters, may generalize better than C2FAR. Also, given it has extra hyperparameters (number of levels/bins-per-level), and given tuning search space grows exponentially with added hyperparameters, C2FAR may not discover optimum settings as quickly. We investigate experimentally whether the benefits of C2FAR outweigh these drawbacks on real-world data (§5.2).

C2FAR is more *complex* than flat binning, but whether it is less *efficient* depends on implementation. Compared to their 2-level coarse-to-fine model, WaveRNN [35] found flat binning required “significantly more parameters, memory and compute.” We find C2FAR to run slower, but with less memory (Tables 9 and 10 in the supplemental). If flat binning was truly more efficient, we could always generate a large volume of data from a C2FAR model and *uptrain* [11, 50] a flat model on it.

Broader impact. By enabling simultaneous modeling of discrete and continuous series, without human involvement, C2FAR is a step toward a universal forecast model. Large C2FAR models could be trained on vast quantities of diverse series (similar to efforts in text [18, 41, 78] and vision [62, 66, 31]). Such models could be fine-tuned for new domains, and help make highly-accurate forecasting systems more widely-used, improving decision making and resource allocation.

There are also risks to this approach. Very large models have environmental and financial costs [4], which may be unnecessary when smaller models suffice. A universal model may be used more easily by those with less expertise and this may lead to misuse; for example, *automation bias* has been shown to disproportionately affect those with less domain expertise [10]. Recommended usage and possible misuse should be documented through artifacts such as model cards [45] and datasheets [27].

³From a discretization perspective, the optimal K is 2, as rather than a softmax, we may use a logistic function thresholded at 0.5 to select high vs. low bins, only computing $\log_2(I)$ total outputs. However, complexity also depends on the neural architecture. As C2FAR-RNN operates B separate RNNs, it is more efficient to use a higher value of K (but not so high that computing output probabilities dominates) and a lower value of B .

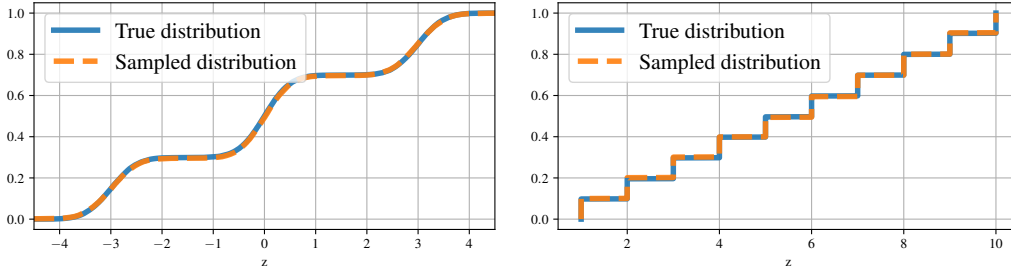


Figure 5: Distribution recovery: CDFs for a Gaussian mixture (left) and discrete uniform over $1 \dots 10$ (right). After training C2FAR-RNNs on each, we sample paths and plot the *sampled* CDF. C2FAR recovers the true CDF much better than SQF-RNN or IQN-RNN (cf. Fig. 3 in [26], Fig. 2 in [30]).

5 Experiments

C2FAR is implemented in PyTorch [49], using a 2-layer LSTM [32] with intra-layer dropout [64, 42], trained via Adam [36]. Notation C2FAR-RNN_B refers to a B-level C2FAR model. We evaluate:

- C2FAR-RNN₁: essentially the standard flat-binning approach [51], but with Pareto tails [21]
- C2FAR-RNN₂: a two-level C2FAR-RNN model
- C2FAR-RNN₃: a three-level C2FAR-RNN model

5.1 Distribution recovery from synthetic data

We first evaluate C2FAR-RNN’s ability to recover the distribution of synthetic data, following [26, 30]. We generate data exactly as in [26], creating 500 series with a year’s worth of hourly observations, each value sampled independently from a 3-component Gaussian mixture with weights $[0.3, 0.4, 0.3]$, means $[-3, 0, 3]$ and standard deviation of 0.4. To illustrate C2FAR-RNN’s ability to model discrete data, we create an equivalent dataset where every element is drawn from a discrete uniform, $\mathcal{U}\{1, 10\}$.

On each dataset, we trained a C2FAR-RNN₃ model with 20 bins per level and hyperparameters based on *elec* experiments (below).

Results. In prior work, SQF-RNN [26] and IQN-RNN [30] struggled to recover the Gaussian mixture, but C2FAR can fit both distributions perfectly (Fig. 5). C2FAR is evidently the state-of-the-art in capturing complex, multi-modal densities without any prior information.

5.2 Empirical study on real-world data

Datasets. We evaluate C2FAR forecasting models on the following datasets:

- *elec*: hourly electricity usage of 321 customers [19], using *discretized* version from [37].
- *traff*: real-valued hourly occupancy from 0 to 1 for 862 car lanes [19], using version from [79].
- *wiki*, daily integer number of hits for 9535 pages, first used in [26], using same version as in [30].
- *azure*, (discrete) hourly usage of virtual machine (VM) flavors and flavor groupings (by tenant, deployment type, etc., in units of VCPUs or GB of memory) in a large public cloud, based on data from [17]. We release this dataset publicly as a paper supplement (see supplementary §C.1 for further details).

For *azure*, we use 20 days as training, 3 days for validation, and 3 final days for testing. Other splits are as in [56]. We forecast 24 hours for hourly series, 30 days for *wiki*, and use rolling evals as in [30].

Metrics. To evaluate point forecasts, we output the median of our forecast distribution and compute *normalized deviation* (ND) from true values. We evaluate probabilistic forecasts using *weighted quantile loss* (wQL), evaluated at forecast quantiles $\{0.1, 0.2 \dots 0.9\}$, as in [51]. For non-probabilistic baselines Naïve and Seasonal-naïve (described below), note wQL reduces to ND, similarly to how

Table 1: ND, wQL, Cov80, and Cov99 for our implementations (top), results from [51] (middle, denoted †) and [30] (bottom, denoted ‡), where available. In all cases, flat binned C2FAR-RNN₁ improves on DeepAR-Gaussian, while deeper C2FAR-RNN₂ likewise improves over C2FAR-RNN₁. Results are generally superior to prior state-of-the-art output distributions in RNN-based forecasting.

	ND%				wQL%				Cov80%	Cov99%
	<i>elec</i>	<i>traff</i>	<i>wiki</i>	<i>azure</i>	<i>elec</i>	<i>traff</i>	<i>wiki</i>	<i>azure</i>	<i>azure</i>	<i>azure</i>
Naïve	40.8	73.6	35.7	3.49	40.8	73.6	35.7	3.49	-	-
Seasonal-naïve	6.97	25.1	33.2	3.67	6.97	25.1	33.2	3.67	-	-
ETS	8.61	33.3	34.3	3.46	8.40	31.5	32.5	2.97	85.5/10.5	96.3/20.3
DeepAR-Gaussian	7.05	16.1	43.8	3.60	5.60	13.7	54.7	3.06	89.9/16.9	98.0/37.7
C2FAR-RNN ₁	6.14	13.0	24.6	2.95	4.87	10.7	21.3	2.41	83.6/8.3	98.5/32.2
C2FAR-RNN ₂	6.09	12.9	24.2	2.86	4.83	10.6	21.0	2.31	79.0/8.5	98.4/29.1
C2FAR-RNN ₃	6.00	13.3	24.1	2.77	4.76	10.9	21.0	2.27	86.0/8.9	98.6/32.7
DeepAR-Binned†	8.21	23.2	94.6	-	6.47	18.8	84.7	-	-	-
DeepAR-StudentT†	6.95	14.6	26.9	-	5.71	12.2	23.8	-	-	-
IQN-RNN‡	7.40	16.8	24.1	-	-	-	-	-	-	-
SQF-RNN‡	9.70	18.6	32.8	-	-	-	-	-	-	-
DeepAR-StudentT‡	7.80	21.6	27.0	-	-	-	-	-	-	-

CRPS reduces to absolute error [29, §4.2]. We also test the *calibration* and *sharpness* [74] of each system, measuring coverage of true values within particular percentiles (e.g. from 10% to 90%, coverage closer to 80% is better) and normalized width of this interval (lower is better). For a target coverage of X%, we refer to these metrics together as *CovX* (e.g. Cov80). Scores at extreme percentiles (e.g., Cov99%) help evaluate modeling of distribution tails.

Baselines. We compare our model to the following baselines:

- Naïve [34]: outputs the last-observed historical value at all forecast horizons
- Seasonal-naïve [34]: at each horizon, outputs the value at the most-recently-observed *season* matching the season at that horizon. We thus output the value at the most-recently-observed matching hour-of-day for hourly series, and matching day-of-week for the daily dataset (*wiki*).
- ETS [33]: probabilistic state space models based on exponential smoothing, as implemented in `statsmodels` [58]. For each dataset, we tune (on validation data) whether to include *seasonality* and *trend* (*damped* or *undamped*) terms, and whether to use *estimated* or *heuristic* initialization.
- DeepAR-Gaussian: our implementation of DeepAR with a Gaussian output distribution; Gaussian outputs are common in practice, even on discrete data [39, 57, 15]

Tuning. Deeper C2FAR models include shallower models as special cases. We therefore address the question: does C2FAR’s improved modeling outweigh the wider tuning required? For fair comparison, we establish a *parameter budget* [42] of 1M parameters; after sampling other hyperparameters, we restrict the possible number of LSTM hidden units so that this cap is enforced. We also restrict the number of tuning trials (on validation data) to 100 for each system.⁴ We tune directly for normalized deviation via Optuna [1], with TPESampler [9], using MedianPruning and early stopping.

Results. Table 1 confirms that deeper C2FAR models improve over flat binnings. In only one case (*traff*) did a C2FAR model not improve over flat binning. In this case, C2FAR-RNN₃, with a larger tuning search space, also failed to find a superior setting of hyperparameters on validation data; going forward, using the same number of bins at each level (i.e., a constant *K*) could enable deeper C2FAR models without additional tuning. Contrary to prior work, we also find flat binning much more effective than standard parametric distributions. We attribute this difference to our use of systematic tuning; prior work used a fixed 1024 bins [51], while our tuner often selected quite fewer bins for C2FAR-RNN₁ (supplemental Table 7). In terms of both standard and extreme percentiles (Cov80% and Cov99% in Table 1), we find C2FAR models are both better calibrated than DeepAR-Gaussian (being twice as close to the desired coverage) while also having a sharper prediction interval width.

⁴In the prior work that mentions hyperparameter tuning, it is common to compare systems tuned with a fixed number of tuning trials, whether as part of grid search [80, 81, 53, 56] or other procedure (e.g., hyperopt in [13], random search in [40]). Training times are on the same order for all our trained systems (supplemental Table 8).

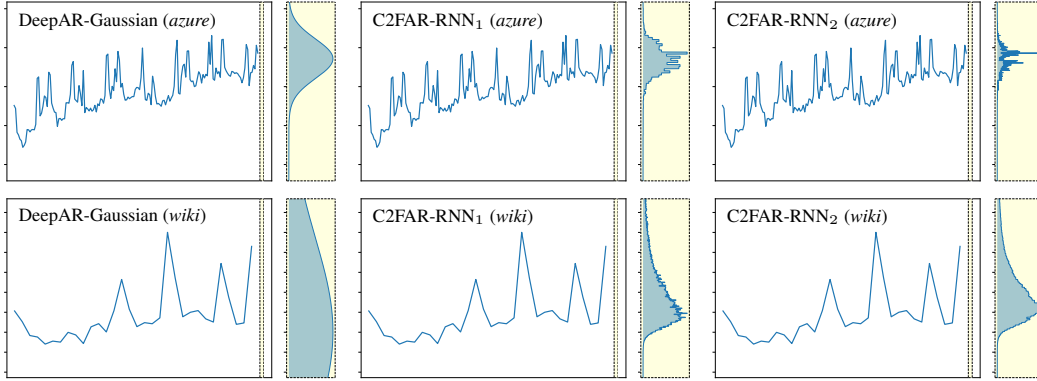


Figure 6: Distributions over possible next values. To cover likely values, Gaussians (left) also cover many unlikely ones. Flat binnings (middle) are optimized to either use fewer bins, but suffer in precision (top), or many bins but suffer in noise (bottom). C2FAR-RNN₂ (right) is able to place high probability on a repeat of the previous value (top) or generate smooth distributions (bottom).

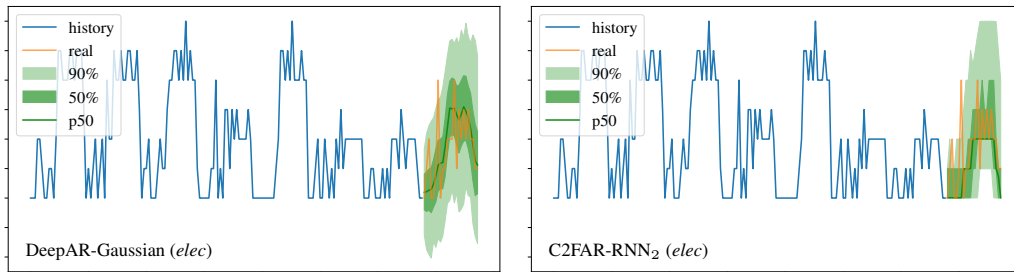


Figure 7: Forecast for an *elec* time series. DeepAR-Gaussian (left) yields a reasonable p50, but its lower percentiles span too low. C2FAR-RNN₂ yields better lower quantiles. C2FAR percentiles also suggest high-fidelity roll-outs, i.e., samples that closely mimic the discretized dynamics of the series.

Seasonal-naïve is surprisingly competitive with DeepAR-Gaussian (except on *traff*, which has both daily and weekly seasonality). This has been observed previously (e.g., Table 1 in [2]); indeed, one of the authors of DeepAR and GluonTS has remarked that “a seasonal naïve model performs almost as well as DeepAR or other deep models on [*elec* and *traff*], and without additional covariates, I suspect it’s almost impossible to perform significantly better in terms of point predictions” [25]. But our results show that C2FAR *can* significantly improve over DeepAR and Seasonal-naïve without using additional covariates, but rather with a better output model.

Analyzing the distributions, we find C2FAR models are able to achieve good *precision* (having many intervals), while simultaneously learning smooth distributions (Fig. 6). Flat binnings must first *learn* “that a value of 128 is close to a value of 127 or 129” [55], while for C2FAR models, intervals will implicitly be close in probability because they are in the same coarser bins.

Autoregressive models have a known disconnect between training, when true values are used as autoregressive inputs, and generation, when samples are used [5]. Our results suggest that such error accumulation may be especially problematic when a model is trained on discrete or mixed data, but uses standard continuous parametric outputs (as in DeepAR-Gaussian). Precise C2FAR models not only provide better forecast quantiles, they enable higher-fidelity samples to be recursively fed back in as autoregressive inputs (Fig. 7). Analyzing error by forecast horizon (supplemental §C.8), we find that at shorter horizons, DeepAR-Gaussian often performs similarly to C2FAR, but at later horizons, the gap widens. So while other solutions to error accumulation exist [67, 74, 76], one effective approach is evidently to generate and recurse on higher-fidelity outputs using C2FAR.

6 Conclusion

We presented C2FAR, a new method for density modeling. C2FAR reduces the generative process to a sequence of classifications over a hierarchical, discretized representation, with special handling of data outside the binning range. C2FAR can be applied to a variety of neural architectures, including RNN-based probabilistic forecasting, where it achieves state-of-the-art results when recovering synthetic distributions and forecasting real-world data. We show binned models (whether flat or, especially, coarse-to-fine) are superior to standard distributions — if binning precision is tuned.

Analysis shows that C2FAR can successfully model complex, multi-modal densities, in real or discrete data, without any prior information. This flexibility enables improved modeling for a variety of time series use cases, including forecasting, anomaly detection, interpolation, compression, denoising, and generating high-fidelity samples. It also enables development of large-scale forecasting models trained on diverse datasets, i.e., it is a step toward a universal neural forecaster.

References

- [1] Takuya Akiba, Shotaro Sano, Toshihiko Yanase, Takeru Ohta, and Masanori Koyama. 2019. Optuna: A Next-generation Hyperparameter Optimization Framework. In *ACM SIGKDD International Conference on Knowledge Discovery & Data Mining*. 2623–2631.
- [2] Alexander Alexandrov, Konstantinos Benidis, Michael Bohlke-Schneider, Valentin Flunkert, Jan Gasthaus, Tim Januschowski, Danielle C Maddix, Syama Rangapuram, David Salinas, Jasper Schulz, Stella Lorenzo, Ali Caner Türkmen, and Yuyang Wang. 2020. GluonTS: Probabilistic and Neural Time Series Modeling in Python. *Journal of Machine Learning Research* 21, 116 (2020), 1–6.
- [3] Dzmitry Bahdanau, Kyunghyun Cho, and Yoshua Bengio. 2015. Neural Machine Translation by Jointly Learning to Align and Translate. *International Conference on Learning Representation* (2015).
- [4] Emily M Bender, Timnit Gebru, Angelina McMillan-Major, and Shmargaret Shmitchell. 2021. On the Dangers of Stochastic Parrots: Can Language Models Be Too Big?. In *ACM Conference on Fairness, Accountability, and Transparency*. 610–623.
- [5] Samy Bengio, Oriol Vinyals, Navdeep Jaitly, and Noam Shazeer. 2015. Scheduled Sampling for Sequence Prediction with Recurrent Neural Networks. *Advances in Neural Information Processing Systems* 28 (2015).
- [6] Yoshua Bengio and Samy Bengio. 2000. Modeling High-Dimensional Discrete Data with Multi-Layer Neural Networks. In *Advances in Neural Information Processing Systems*.
- [7] Konstantinos Benidis, Syama Sundar Rangapuram, Valentin Flunkert, Yuyang Wang, Danielle Maddix, Caner Turkmen, Jan Gasthaus, Michael Bohlke-Schneider, David Salinas, Lorenzo Stella, François-Xavier Aubet, Laurent Callot, and Tim Januschowski. 2022. Deep Learning for Time Series Forecasting: Tutorial and Literature Survey. *Comput. Surveys* (2022).
- [8] Shane Bergsma, Timothy Zeyl, Arik Senderovich, and J Christopher Beck. 2021. Generating Complex, Realistic Cloud Workloads using Recurrent Neural Networks. In *ACM SIGOPS Symposium on Operating Systems Principles*. 376–391.
- [9] James Bergstra, Rémi Bardenet, Yoshua Bengio, and Balázs Kégl. 2011. Algorithms for Hyper-Parameter Optimization. *Advances in Neural Information Processing Systems* 24 (2011).
- [10] Raymond R Bond, Tomas Novotny, Irena Andrsova, Lumir Koc, Martina Sisakova, Dewar Finlay, Daniel Guldenring, James McLaughlin, Aaron Peace, Victoria McGilligan, Stephen J. Leslie, Hui Wang, and Marek Malik. 2018. Automation bias in medicine: The influence of automated diagnoses on interpreter accuracy and uncertainty when reading electrocardiograms. *Journal of Electrocardiology* 51, 6 (2018), S6–S11.
- [11] Cristian Buciluă, Rich Caruana, and Alexandru Niculescu-Mizil. 2006. Model Compression. In *ACM SIGKDD International Conference on Knowledge Discovery & Data Mining*. 535–541.

- [12] Defu Cao, Yujing Wang, Juanyong Duan, Ce Zhang, Xia Zhu, Congrui Huang, Yunhai Tong, Bixiong Xu, Jing Bai, Jie Tong, and Qi Zhang. 2020. Spectral Temporal Graph Neural Network for Multivariate Time-series Forecasting. *Advances in Neural Information Processing Systems* 33 (2020).
- [13] Cristian Challu, Kin G Olivares, Boris N Oreshkin, Federico Garza, Max Mergenthaler, and Artur Dubrawski. 2022. N-HiTS: Neural Hierarchical Interpolation for Time Series Forecasting. *arXiv preprint arXiv:2201.12886* (2022).
- [14] Nicolas Chapados. 2014. Effective Bayesian Modeling of Groups of Related Count Time Series. In *International Conference on Machine Learning*. 1395–1403.
- [15] Yitian Chen, Yanfei Kang, Yixiong Chen, and Zizhuo Wang. 2020. Probabilistic Forecasting with Temporal Convolutional Neural Network. *Neurocomputing* 399 (2020), 491–501.
- [16] Jonathan H Clark, Chris Dyer, Alon Lavie, and Noah A Smith. 2011. Better Hypothesis Testing for Statistical Machine Translation: Controlling for Optimizer Instability. In *Annual Meeting of the Association for Computational Linguistics: Human Language Technologies*. 176–181.
- [17] Eli Cortez, Anand Bonde, Alexandre Muzio, Mark Russinovich, Marcus Fontoura, and Ricardo Bianchini. 2017. Resource Central: Understanding and Predicting Workloads for Improved Resource Management in Large Cloud Platforms. In *Symposium on Operating Systems Principles*. 153–167.
- [18] Jacob Devlin, Ming-Wei Chang, Kenton Lee, and Kristina Toutanova. 2018. BERT: Pre-training of Deep Bidirectional Transformers for Language Understanding. *arXiv preprint arXiv:1810.04805* (2018).
- [19] Dheeru Dua and Casey Graff. 2017. UCI Machine Learning Repository. <http://archive.ics.uci.edu/ml>
- [20] Conor Durkan, Artur Bekasov, Iain Murray, and George Papamakarios. 2019. Neural Spline Flows. *Advances in Neural Information Processing Systems* 32 (2019).
- [21] Elena Ehrlich, Laurent Callot, and François-Xavier Aubet. 2021. Spliced Binned-Pareto Distribution for Robust Modeling of Heavy-tailed Time Series. *arXiv preprint arXiv:2106.10952* (2021).
- [22] Chenyou Fan, Yuze Zhang, Yi Pan, Xiaoyue Li, Chi Zhang, Rong Yuan, Di Wu, Wensheng Wang, Jian Pei, and Heng Huang. 2019. Multi-Horizon Time Series Forecasting with Temporal Attention Learning. In *ACM SIGKDD International Conference on Knowledge Discovery & Data Mining*. 2527–2535.
- [23] Usama Fayyad and Keki Irani. 1993. Multi-Interval Discretization of Continuous-Valued Attributes for Classification Learning. *International Joint Conference On Artificial Intelligence* 2 (1993), 1022–1027.
- [24] Brendan J Frey, Geoffrey E Hinton, and Peter Dayan. 1995. Does the Wake-sleep Algorithm Produce Good Density Estimators? *Advances in Neural Information Processing Systems* 8 (1995).
- [25] Jan Gasthaus. 2020. Re: A Worrying Analysis of Probabilistic Time-series Models for Sales Forecasting [discussion comment]. <https://github.com/aws-labs/gluonts/discussions/1180?sort=new?sort=new#discussioncomment-169433> Posted: 2020-11-30, Accessed: 2022-09-13.
- [26] Jan Gasthaus, Konstantinos Benidis, Yuyang Wang, Syama Sundar Rangapuram, David Salinas, Valentin Flunkert, and Tim Januschowski. 2019. Probabilistic Forecasting with Spline Quantile Function RNNs. In *International Conference on Artificial Intelligence and Statistics*. 1901–1910.
- [27] Timnit Gebru, Jamie Morgenstern, Briana Vecchione, Jennifer Wortman Vaughan, Hanna Wallach, Hal Daumé III, and Kate Crawford. 2021. Datasheets for Datasets. *Commun. ACM* 64, 12 (2021), 86–92.

- [28] Mathieu Germain, Karol Gregor, Iain Murray, and Hugo Larochelle. 2015. MADE: Masked Autoencoder for Distribution Estimation. In *International Conference on Machine Learning*. 881–889.
- [29] Tilmann Gneiting and Adrian E Raftery. 2007. Strictly Proper Scoring Rules, Prediction, and Estimation. *J. Amer. Statist. Assoc.* 102, 477 (2007), 359–378.
- [30] Adèle Gouttes, Kashif Rasul, Mateusz Koren, Johannes Stephan, and Tofigh Naghibi. 2021. Probabilistic Time Series Forecasting with Implicit Quantile Networks. *arXiv preprint arXiv:2107.03743* (2021).
- [31] Kaiming He, Xiangyu Zhang, Shaoqing Ren, and Jian Sun. 2016. Deep Residual Learning for Image Recognition. In *IEEE Conference on Computer Vision and Pattern Recognition*. 770–778.
- [32] Sepp Hochreiter and Jürgen Schmidhuber. 1997. Long Short-Term Memory. *Neural computation* 9, 8 (1997), 1735–1780.
- [33] Rob Hyndman, Anne B Koehler, J Keith Ord, and Ralph D Snyder. 2008. *Forecasting with Exponential Smoothing: The State Space Approach*. Springer Science & Business Media.
- [34] Rob J Hyndman and George Athanasopoulos. 2018. *Forecasting: Principles and Practice*. OTexts.
- [35] Nal Kalchbrenner, Erich Elsen, Karen Simonyan, Seb Noury, Norman Casagrande, Edward Lockhart, Florian Stimberg, Aaron van den Oord, Sander Dieleman, and Koray Kavukcuoglu. 2018. Efficient Neural Audio Synthesis. In *International Conference on Machine Learning*. 2410–2419.
- [36] Diederik P Kingma and Jimmy Ba. 2014. Adam: A Method for Stochastic Optimization. *arXiv preprint arXiv:1412.6980* (2014).
- [37] Guokun Lai, Wei-Cheng Chang, Yiming Yang, and Hanxiao Liu. 2018. Modeling Long-and Short-Term Temporal Patterns with Deep Neural Networks. In *ACM SIGIR Conference on Research & Development in Information Retrieval*. 95–104.
- [38] Hugo Larochelle and Iain Murray. 2011. The Neural Autoregressive Distribution Estimator. In *International Conference on Artificial Intelligence and Statistics*. JMLR Workshop and Conference Proceedings, 29–37.
- [39] Shiyang Li, Xiaoyong Jin, Yao Xuan, Xiyu Zhou, Wenhui Chen, Yu-Xiang Wang, and Xifeng Yan. 2019. Enhancing the Locality and Breaking the Memory Bottleneck of Transformer on Time Series Forecasting. *Advances in Neural Information Processing Systems* 32 (2019).
- [40] Bryan Lim, Serkan Ö Arık, Nicolas Loeff, and Tomas Pfister. 2021. Temporal Fusion Transformers for Interpretable Multi-Horizon Time Series Forecasting. *International Journal of Forecasting* 37, 4 (2021), 1748–1764.
- [41] Yinhan Liu, Myle Ott, Naman Goyal, Jingfei Du, Mandar Joshi, Danqi Chen, Omer Levy, Mike Lewis, Luke Zettlemoyer, and Veselin Stoyanov. 2019. Roberta: A Robustly Optimized BERT Pretraining Approach. *arXiv preprint arXiv:1907.11692* (2019).
- [42] Gábor Melis, Chris Dyer, and Phil Blunsom. 2017. On the State of the Art of Evaluation in Neural Language Models. *arXiv preprint arXiv:1707.05589* (2017).
- [43] Tomas Mikolov, Kai Chen, Greg Corrado, and Jeffrey Dean. 2013. Efficient Estimation of Word Representations in Vector Space. *arXiv preprint arXiv:1301.3781* (2013).
- [44] Yongyi Min and Alan Agresti. 2002. Modeling Nonnegative Data with Clumping at Zero: A Survey. *Journal of the Iranian Statistical Society (JIRSS)* (2002).
- [45] Margaret Mitchell, Simone Wu, Andrew Zaldivar, Parker Barnes, Lucy Vasserman, Ben Hutchinson, Elena Spitzer, Inioluwa Deborah Raji, and Timnit Gebru. 2019. Model Cards for Model Reporting. In *Conference on Fairness, Accountability, and Transparency*. 220–229.

- [46] Andriy Mnih and Geoffrey Hinton. 2008. A Scalable Hierarchical Distributed Language Model. *Advances in Neural Information Processing Systems* 21 (2008).
- [47] Frederic Morin and Yoshua Bengio. 2005. Hierarchical Probabilistic Neural Network Language Model. In *International Workshop on Artificial Intelligence and Statistics*. 246–252.
- [48] Srayanta Mukherjee, Devashish Shankar, Atin Ghosh, Nilam Tathawadekar, Pramod Kompalli, Sunita Sarawagi, and Krishnendu Chaudhury. 2018. AR-MDN: Associative and Recurrent Mixture Density Networks for eRetail Demand Forecasting. *arXiv preprint arXiv:1803.03800* (2018).
- [49] Adam Paszke, Sam Gross, Francisco Massa, Adam Lerer, James Bradbury, Gregory Chanan, Trevor Killeen, Zeming Lin, Natalia Gimelshein, Luca Antiga, Alban Desmaison, Andreas Köpf, Edward Yang, Zach DeVito, Martin Raison, Tejani Alykhan, Sasank Chilamkurthy, Benoit Steiner, Lu Fang, Junjie Bai, and Soumith Chintala. 2019. PyTorch: An Imperative Style, High-Performance Deep Learning Library. *Advances in Neural Information Processing Systems* 32 (2019).
- [50] Slav Petrov, Pi-Chuan Chang, Michael Ringgaard, and Hiyan Alshawi. 2010. Uptraining for Accurate Deterministic Question Parsing. In *Empirical Methods in Natural Language Processing*. 705–713.
- [51] Stephan Rabanser, Tim Januschowski, Valentin Flunkert, David Salinas, and Jan Gasthaus. 2020. The Effectiveness of Discretization in Forecasting: An Empirical Study on Neural Time Series Models. *arXiv preprint arXiv:2005.10111* (2020).
- [52] Maithra Raghu, Ben Poole, Jon Kleinberg, Surya Ganguli, and Jascha Sohl-Dickstein. 2017. On the Expressive Power of Deep Neural Networks. In *International Conference on Machine Learning*. 2847–2854.
- [53] Syama Sundar Rangapuram, Lucien D Werner, Konstantinos Benidis, Pedro Mercado, Jan Gasthaus, and Tim Januschowski. 2021. End-to-End Learning of Coherent Probabilistic Forecasts for Hierarchical Time Series. In *International Conference on Machine Learning*. 8832–8843.
- [54] Kashif Rasul, Abdul-Saboor Sheikh, Ingmar Schuster, Urs Bergmann, and Roland Vollgraf. 2020. Multi-Variate Probabilistic Time Series Forecasting via Conditioned Normalizing Flows. *arXiv preprint arXiv:2002.06103* (2020).
- [55] Tim Salimans, Andrej Karpathy, Xi Chen, and Diederik P Kingma. 2017. PixelCNN++: Improving the PixelCNN with Discretized Logistic Mixture Likelihood and other Modifications. *arXiv preprint arXiv:1701.05517* (2017).
- [56] David Salinas, Michael Bohlke-Schneider, Laurent Callot, Roberto Medico, and Jan Gasthaus. 2019. High-Dimensional Multivariate Forecasting with Low-Rank Gaussian Copula Processes. *Advances in Neural Information Processing Systems* 32 (2019).
- [57] David Salinas, Valentin Flunkert, Jan Gasthaus, and Tim Januschowski. 2020. DeepAR: Probabilistic Forecasting with Autoregressive Recurrent Networks. *International Journal of Forecasting* 36, 3 (2020), 1181–1191.
- [58] Skipper Seabold and Josef Perktold. 2010. Statsmodels: Econometric and Statistical Modeling with Python. In *9th Python in Science Conference*. 92–96.
- [59] Matthias W Seeger, David Salinas, and Valentin Flunkert. 2016. Bayesian Intermittent Demand Forecasting for Large Inventories. *Advances in Neural Information Processing Systems* 29 (2016).
- [60] Rajat Sen, Hsiang-Fu Yu, and Inderjit Dhillon. 2019. Think Globally, Act Locally: A Deep Neural Network Approach to High-Dimensional Time Series Forecasting. *arXiv preprint arXiv:1905.03806* (2019).
- [61] Jin Shieh and Eamonn Keogh. 2008. iSAX: Indexing and Mining Terabyte Sized Time Series. In *ACM SIGKDD International Conference on Knowledge Discovery & Data Mining*. 623–631.

- [62] Karen Simonyan and Andrew Zisserman. 2014. Very Deep Convolutional Networks for Large-Scale Image Recognition. *arXiv preprint arXiv:1409.1556* (2014).
- [63] Ralph D Snyder, J Keith Ord, and Adrian Beaumont. 2012. Forecasting the intermittent demand for slow-moving inventories: A modelling approach. *International Journal of Forecasting* 28, 2 (2012), 485–496.
- [64] Nitish Srivastava, Geoffrey Hinton, Alex Krizhevsky, Ilya Sutskever, and Ruslan Salakhutdinov. 2014. Dropout: A Simple Way to Prevent Neural Networks from Overfitting. *Journal of Machine Learning Research* 15, 1 (2014), 1929–1958.
- [65] Ilya Sutskever, Oriol Vinyals, and Quoc V Le. 2014. Sequence to Sequence Learning with Neural Networks. In *Advances in Neural Information Processing Systems*, Vol. 27.
- [66] Christian Szegedy, Wei Liu, Yangqing Jia, Pierre Sermanet, Scott Reed, Dragomir Anguelov, Dumitru Erhan, Vincent Vanhoucke, and Andrew Rabinovich. 2015. Going Deeper with Convolutions. In *IEEE Conference on Computer Vision and Pattern Recognition*. 1–9.
- [67] Souhaib Ben Taieb and Amir F Atiya. 2015. A Bias and Variance Analysis for Multistep-Ahead Time Series Forecasting. *IEEE Transactions on Neural Networks and Learning Systems* 27, 1 (2015), 62–76.
- [68] Souhaib Ben Taieb, James W Taylor, and Rob J Hyndman. 2017. Coherent Probabilistic Forecasts for Hierarchical Time Series. In *International Conference on Machine Learning*. 3348–3357.
- [69] Lucas Theis, Aäron van den Oord, and Matthias Bethge. 2015. A note on the evaluation of generative models. *arXiv preprint arXiv:1511.01844* (2015).
- [70] Benigno Urias, Marc-Alexandre Côté, Karol Gregor, Iain Murray, and Hugo Larochelle. 2016. Neural Autoregressive Distribution Estimation. *Journal of Machine Learning Research* 17, 1 (2016), 7184–7220.
- [71] Benigno Urias, Iain Murray, and Hugo Larochelle. 2013. RNADE: The real-valued neural autoregressive density-estimator. *Advances in Neural Information Processing Systems* 26 (2013).
- [72] Aaron van den Oord, Nal Kalchbrenner, and Koray Kavukcuoglu. 2016. Pixel Recurrent Neural Networks. In *International Conference on Machine Learning*. 1747–1756.
- [73] Ravichander Vipera, Sangjun Park, Kihyun Choo, Samin Ishtiaq, Kyoungbo Min, Sourav Bhat-tacharya, Abhinav Mehrotra, Alberto Gil CP Ramos, and Nicholas D Lane. 2020. Bunched LPC-Net: Vocoder for Low-Cost Neural Text-To-Speech Systems. *arXiv preprint arXiv:2008.04574* (2020).
- [74] Ruofeng Wen, Kari Torkkola, Balakrishnan Narayanaswamy, and Dhruv Madeka. 2017. A Multi-Horizon Quantile Recurrent Forecaster. *arXiv preprint arXiv:1711.11053* (2017).
- [75] Haixu Wu, Jiehui Xu, Jianmin Wang, and Mingsheng Long. 2021. Autoformer: Decomposition Transformers with Auto-Correlation for Long-Term Series Forecasting. *Advances in Neural Information Processing Systems* 34 (2021).
- [76] Sifan Wu, Xi Xiao, Qianggang Ding, Peilin Zhao, Ying Wei, and Junzhou Huang. 2020. Adversarial Sparse Transformer for Time Series Forecasting. *Advances in Neural Information Processing Systems* 33 (2020), 17105–17115.
- [77] Tsun-Yi Yang, Yi-Hsuan Huang, Yen-Yu Lin, Pi-Cheng Hsiu, and Yung-Yu Chuang. 2018. SSR-Net: A Compact Soft Stagewise Regression Network for Age Estimation. In *International Joint Conference On Artificial Intelligence*. 1078–1084.
- [78] Zhilin Yang, Zihang Dai, Yiming Yang, Jaime Carbonell, Russ R Salakhutdinov, and Quoc V Le. 2019. XLNet: Generalized Autoregressive Pretraining for Language Understanding. *Advances in Neural Information Processing Systems* 32 (2019).

- [79] Hsiang-Fu Yu, Nikhil Rao, and Inderjit S Dhillon. 2016. Temporal Regularized Matrix Factorization for High-Dimensional Time Series Prediction. *Advances in Neural Information Processing Systems* 29 (2016).
- [80] Haoyi Zhou, Shanghang Zhang, Jieqi Peng, Shuai Zhang, Jianxin Li, Hui Xiong, and Wancai Zhang. 2021. Informer: Beyond Efficient Transformer for Long Sequence Time-Series Forecasting. In *AAAI Conference on Artificial Intelligence*. 11106–11115.
- [81] Zhibo Zhu, Ziqi Liu, Ge Jin, Zhiqiang Zhang, Lei Chen, Jun Zhou, and Jianyong Zhou. 2021. MixSeq: Connecting Macroscopic Time Series Forecasting with Microscopic Time Series Data. *Advances in Neural Information Processing Systems* 34 (2021).

Checklist

1. For all authors...
 - (a) Do the main claims made in the abstract and introduction accurately reflect the paper’s contributions and scope? [Yes]
 - (b) Did you describe the limitations of your work? [Yes] In particular, §4.3
 - (c) Did you discuss any potential negative societal impacts of your work? [Yes] §4.3
 - (d) Have you read the ethics review guidelines and ensured that your paper conforms to them? [Yes]
2. If you are including theoretical results...
 - (a) Did you state the full set of assumptions of all theoretical results? [N/A]
 - (b) Did you include complete proofs of all theoretical results? [N/A]
3. If you ran experiments...
 - (a) Did you include the code, data, and instructions needed to reproduce the main experimental results (either in the supplemental material or as a URL)? [No] The full codebase is proprietary, however the core code for C2FAR is shared at https://github.com/huaweicloud/c2far_forecasting. All datasets are either shared as a paper contribution, or already public.
 - (b) Did you specify all the training details (e.g., data splits, hyperparameters, how they were chosen)? [Yes] See §5.2 and paper supplement.
 - (c) Did you report error bars (e.g., with respect to the random seed after running experiments multiple times)? [Yes] See paper supplement.
 - (d) Did you include the total amount of compute and the type of resources used (e.g., type of GPUs, internal cluster, or cloud provider)? [Yes] See paper supplement.
4. If you are using existing assets (e.g., code, data, models) or curating/releasing new assets...
 - (a) If your work uses existing assets, did you cite the creators? [Yes] §5.2
 - (b) Did you mention the license of the assets? [Yes] For shared data, see supplement
 - (c) Did you include any new assets either in the supplemental material or as a URL? [Yes] See paper supplement.
 - (d) Did you discuss whether and how consent was obtained from people whose data you’re using/curating? [Yes] See paper supplement.
 - (e) Did you discuss whether the data you are using/curating contains personally identifiable information or offensive content? [Yes] See paper supplement.
5. If you used crowdsourcing or conducted research with human subjects...
 - (a) Did you include the full text of instructions given to participants and screenshots, if applicable? [N/A]
 - (b) Did you describe any potential participant risks, with links to Institutional Review Board (IRB) approvals, if applicable? [N/A]
 - (c) Did you include the estimated hourly wage paid to participants and the total amount spent on participant compensation? [N/A]

A Experimental details

A.1 Architecture

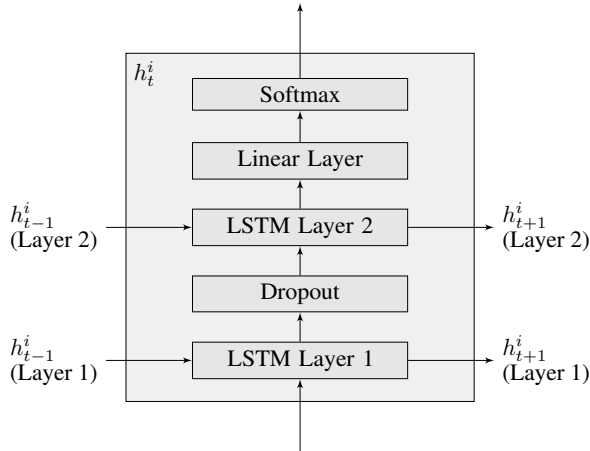


Figure 8: LSTM architecture for h_t^i : one level of C2FAR at time t and level i (see Fig. 4 in main paper). Network layers do include *bias weights*. The same number of hidden units are used in each LSTM layer and is given by hyperparameter n_hidden . Dropout probability is given by hyperparameter $lstm_dropout$.

Regarding the sequence model, all C2FAR-RNN models use 2-layer LSTMs [32] with intra-layer dropout [64, 42], as depicted in Fig. 8. Multi-level C2FAR-RNN models use the same LSTM architecture at each level, with the same number of hidden units in each LSTM layer of each level. We follow DeepAR [57] in using the same network to encode (i.e., process the conditioning range) and decode (i.e., generate values in the prediction range). However, unlike DeepAR, during training we only compute loss over the prediction range.

For generating the parameters of the Pareto distribution, we use a feed-forward neural network with a single hidden layer (followed by a *softplus* output transformation). The number of units in this hidden layer is also controlled by the n_hidden hyperparameter.

A.2 Features and input/output preparation

Toward our goal of universal forecasting (§4.3 of the main paper), we exclude covariates for series-specific meta data, series “age”, and lagged historical values (all of which are used in [57]). We use min-max scaling [51] to normalize conditioning ranges prior to forecasting. Autoregressive inputs are represented with 1-hot-encodings.

A.3 Training and testing details

We use Optuna [1] for tuning, with the TPESampler [9], and use both MedianPruning (pruning unpromising trials compared to previous trials) and early stopping (stopping trials when results no longer improve). We stop early if we see $n_stop_evals_no_improve$ evaluations without a new top score (currently set to 37, see Table 6).

We filter instances with constant *conditioning* ranges from training and testing. We do not oversample training instances from the higher-amplitude series, as DeepAR does [57].

We vectorize across multiple series during both the computing of likelihood (in training) and during the sampling of future values (in prediction). The number of series that we parallelize over is referred to as our “batch size” (e.g. $n_train_batch_size$).

We also vectorize across different multi-step-ahead rollouts during the Monte Carlo procedure to generate the forecast distribution. We use 500 separate rollouts during the forecasting process

Table 2: Negative log likelihood (NLL) of test data for different models on synthetic data

	GMM	Discrete
DeepAR-Gaussian	0.2526	0.2775
C2FAR-RNN ₁	-0.4150	-1.564
C2FAR-RNN ₂	-0.4198	-4.479
C2FAR-RNN ₃	-0.4203	-6.664

($n_{rollouts} = 500$), unless otherwise stated. We compute rolling evaluations with a stride of 1, i.e., we forecast and evaluate over overlapping prediction ranges, as in [30].

A.4 Computational resources

C2FAR is implemented in PyTorch [49], version 1.9.1+cu102. We use GPUs from Nvidia: four Tesla P100 GPUs with 16280MiB and two Tesla K80 GPUs with 11441MiB. To maximize the utilization of the GPUs, we usually ran two trials in parallel on each of the six GPUs, for 12 trials running in parallel in total at any one time for a given tuning study.

B Distribution recovery

Here we expand on the results in §5.1 of the paper, evaluating each of our implemented systems on the task of recovering synthetic distributions.

B.1 Training details

Rather than tuning the models for this (simple) task, we use a fixed learning rate of $2e-2$, a weight decay of $1e-6$, and 64 hidden units, which are settings that worked well during development experiments on the *elec* validation set. We also used an *lstm_dropout* of $1e-3$ and training batch size of 1024 (as in Table 6). The (normalized) binning extent is taken from -0.01 to 1.01. We use a conditioning range of 96 and a prediction range of 24, following [26]. We take the final four days as the testing period.

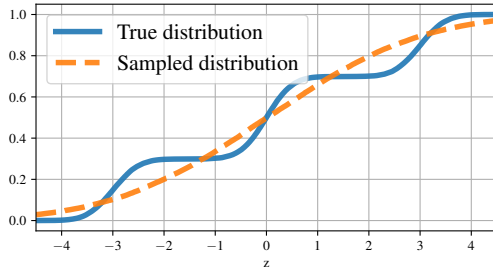
B.2 Computational performance

The time to execute the training runs varied between 53 minutes and 84 minutes for all systems on the synthetic Gaussian Mixture Model (GMM) data, and between 10 minutes and 30 minutes for all systems on the synthetic discrete data.

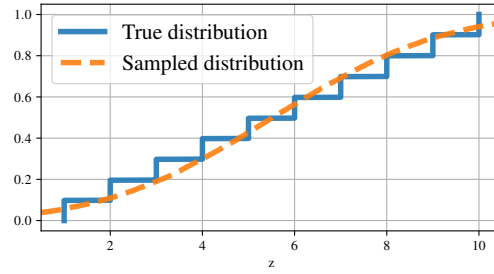
B.3 Further results

Fig. 9 shows the ability of each of our implemented systems to recover the synthetic distribution (repeating the C2FAR-RNN₃ results, also given in Fig. 5 in the main paper). The frequently-used Gaussian output distribution [39, 57, 15] cannot recover the Gaussian mixture since it has only a single mixture component, while it fits the discrete data as well as can be expected. For the C2FAR-RNN models, we use 60 total *bins* across all the levels, which amounts to much greater precision for the multi-level models. Qualitatively, C2FAR-RNN₁ fits the data fairly well, not quite overlapping the true GMM distribution, and struggling to generate the sharp increases in the CDF seen in the discrete data. The C2FAR-RNN₂ and C2FAR-RNN₃ models fit each distribution nearly perfectly.

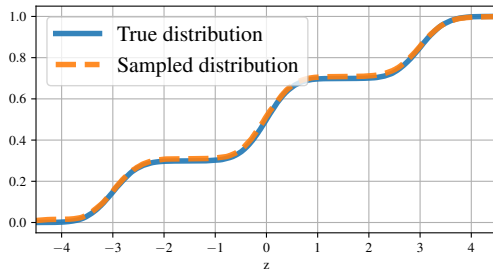
Quantitatively, we can evaluate each of these fits by computing the negative log likelihood (NLL) of the test data, as computed by each model. These results are presented in Table 2, which shows C2FAR-RNN₃ is only very slightly better on GMM, but significantly better on the discrete data. Of course, by adding more layers and bins, we may achieve arbitrarily low NLL on the discrete dataset. Whether such precision is beneficial will depend on the application.



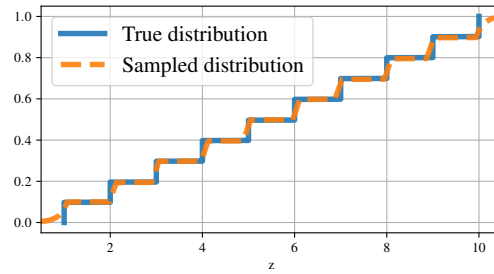
(a) GMM, DeepAR-Gaussian



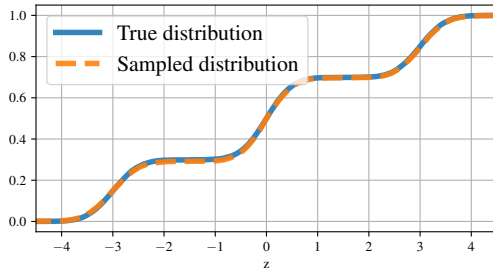
(b) Discrete, DeepAR-Gaussian



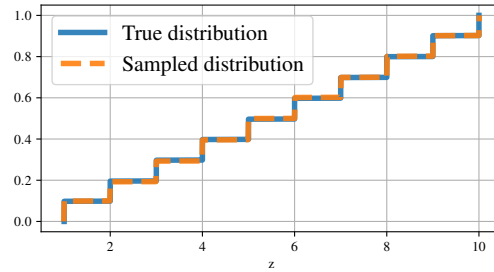
(c) GMM, C2FAR-RNN₁ with 60 bins



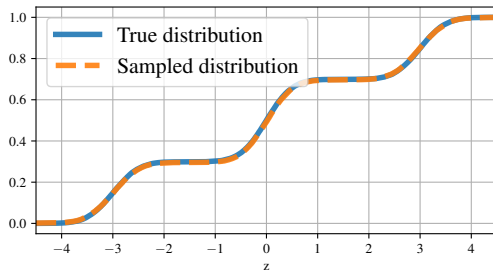
(d) Discrete, C2FAR-RNN₁ with 60 bins



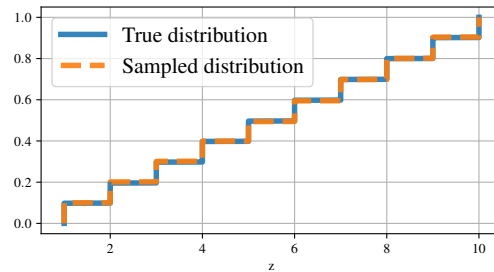
(e) GMM, C2FAR-RNN₂ with 30 + 30 bins



(f) Discrete, C2FAR-RNN₂ with 30 + 30 bins



(g) GMM, C2FAR-RNN₃ with 20 + 20 + 20 bins



(h) Discrete, C2FAR-RNN₃ with 20 + 20 + 20 bins

Figure 9: Distribution recovery supplemental results on the Gaussian mixture model synthetic data (GMM, left) and the discrete uniform synthetic data (Discrete, right) for each of our implemented systems.

Table 3: Information about the *azure* dataset. Flavor *names* are automatically generated from each VM’s allocated *VCPUs* and *Memory* requirement via the template *az-{VCPUs}-{Memory/VCPUs}*. Flavor *types* are defined purely by the Memory:VCPUs ratio via the template *az-{Memory/VCPUs}*.

Duration	30 days
Num. unique VMs	2,013,767
Num. unique subscriptions	5,958, with top 250 used for customer-specific series.
Unique VM categories	{Delay-insensitive, Interactive, Unknown}
Unique flavor names	{az-1-1.75, az-1-2, az-16-7, az-2-1.75, az-2-2, az-2-7, az-2-8, az-4-1.75, az-4-2, az-4-7, az-4-8, az-8-1.75, az-8-2, az-8-7, az-8-8}
Unique flavor types	{az-0.75, az-1.75, az-2, az-7, az-8}

C Empirical study on real-world data: further details

C.1 Azure VM demand dataset

We generated the *azure* dataset in order to provide real-world data reflecting the types of time series seen in the context of large-scale compute clouds. Cloud decision making can benefit from predicted future resource demand, e.g., for capacity planning or scheduling optimization [8]. A dominant workload type in compute clouds is the virtual machine (VM), which is typically available in one of a limited number of specific configurations or *flavors*; essentially, a flavor represents a specific bundle of resource requirements, including VCPU and Memory needs. Forecasts for the total demand (in terms of VCPUs or Memory, in GB) of specific flavors, customers, and workload categories are all valuable. Furthermore, aggregations of these basic time series are also valuable. For example, VM flavors with a common VCPUs:Memory ratio, known as a VM flavor *type*, are often run on shared physical servers, and therefore forecasts of flavor type demand are directly actionable in terms of provisioning of server resources.

We obtained real-world data reflecting these dimensions of cloud resource demand by leveraging the publicly-available *Azure Public Dataset*⁵, originally released in [17] under a Creative Commons Attribution 4.0 International Public License. This dataset contains create, delete, and CPU utilization information (as a % of allocated VCPUs, over time) for over 2 million cloud VMs, reflecting both internal and external customer workload over a 30-day period. We converted this data into time series by counting the total VCPUs and Memory requirements over time for different combinations of flavors, subscriptions (customer IDs), categories, and flavor types, as noted in Table 3. Although we count VMs from all customers, we build customer-specific time series for the top 250 subscription IDs by VM frequency. We also combined lower-level time series to form a hierarchy of time series, as is common in real-world demand data [68, 53]. We also defined a *stopped* VM as any VM whose CPU utilization% drops below 1%. We then created two different versions of our time series, in each case aggregating the data with a 1-hour sampling period:

1. The time series aggregated with the *maximum* of each 1-hour period.
2. The time series aggregated with the *minimum* of each 1-hour period, and excluding stopped VMs at each time point.

In a way, the first set of time series represents a *pessimistic* view of how many resources we require each hour, while the second version represents an *optimistic* view, as we only provision for the minimum and assume we can re-use the resources from stopped VMs.

We provide some examples of these time series in Figs. 10 through 13. Fig. 10 represents the total demand across all VMs, and we can see the strong daily seasonality. Demand of the *delay-insensitive* category, for a particular flavor type, is shown in Fig. 11, while Fig. 12 gives the demand for the same category and flavor type, but for customer 1108 specifically (note all the original IDs are anonymized and represented in the dataset using placeholder values). Demand of the *unknown* category, for flavor name az-8-1.75, is given in Fig. 13.

Although the *azure* dataset covers 30 days, for experiments we use 20 days as training, 3 days for validation, and 3 final days for testing, leaving the remaining few days unseen and available for future experiments.

⁵<https://github.com/Azure/AzurePublicDataset/blob/master/AzurePublicDatasetV1.md>

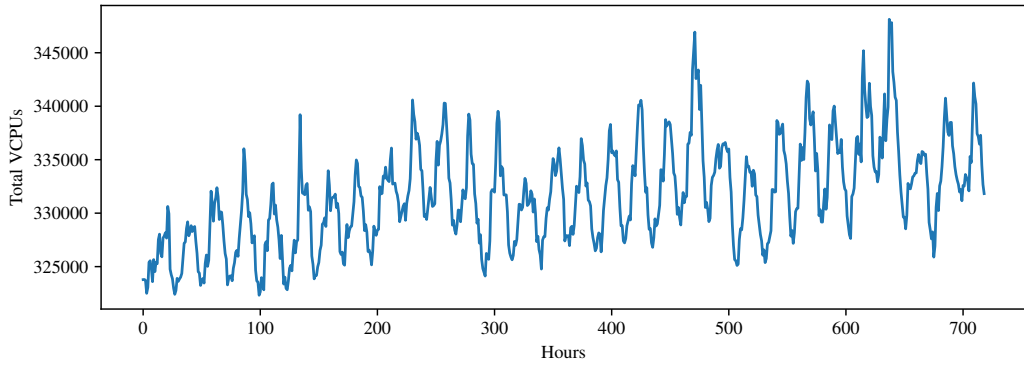


Figure 10: *azure* sample time series: total *aggregate* VCPUs demand. A strong daily seasonality is apparent.

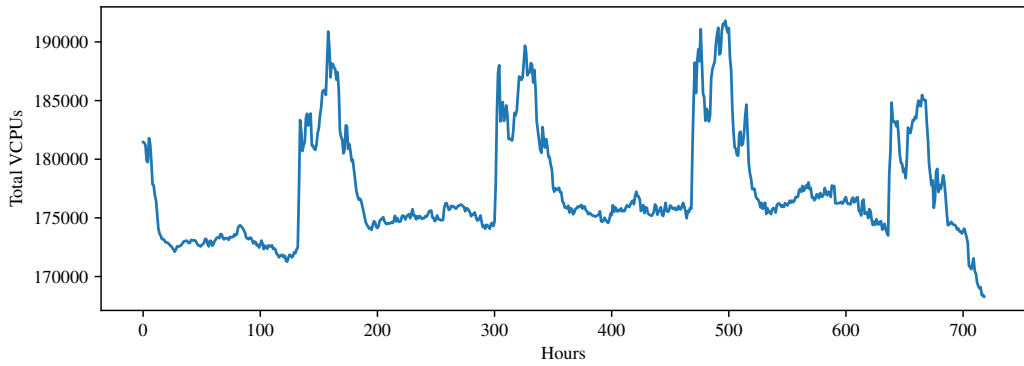


Figure 11: *azure* sample time series: total VCPUs demand of *delay-insensitive* VMs of flavor type *az-1.75*. *Delay-insensitive* VMs exhibit strong weekly seasonality, apparently being used mostly on weekends.

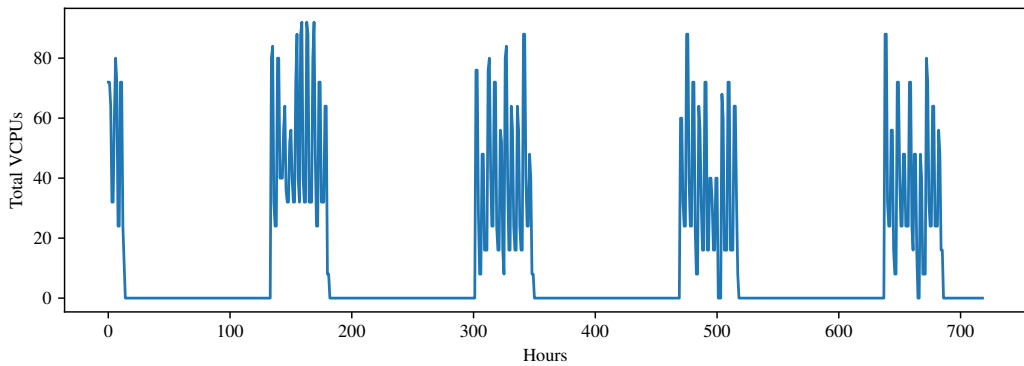


Figure 12: *azure* sample time series: customer 1108, total VCPUs demand of *delay-insensitive* VMs of flavor type *az-1.75*. This particular customer seems to consume resources exclusively on weekends.

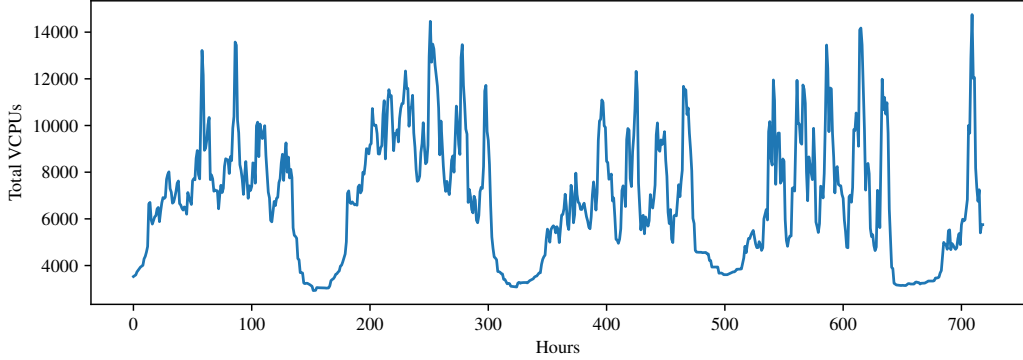


Figure 13: *azure* sample time series: total VCPUs demand of *unknown* VMs of flavor name *az-8-1.75*. *Unknown* VMs exhibit strong daily and weekly seasonality, requiring resources during the periods where *delay-insensitive* VMs are lower (i.e., during weekdays).

Table 4: Dataset details for the empirical study.

Dataset	Binning extent start	Binning extent end	Num. series	Domain	Freq.	Num. vals per series	Num. validation vals per series	Num. test vals per series	Prediction range size
<i>elec</i>	-0.01	1.01	321	Discrete	Hourly	21212	168	168	24
<i>traff</i>	-0.01	1.01	862	Real	Hourly	14204	168	168	24
<i>wiki</i>	-0.2	3.1	9535	Discrete	Daily	912	50	150	30
<i>azure</i>	-0.1	1.3	4098	Discrete	Hourly	719	72	72	24

C.2 Other datasets and dataset details

Beyond *azure*, the *elec*, *traff*, and *wiki* datasets were obtained using scripts in GluonTS [2], with the objective of replicating the training/validation/test splits used in prior work [56, 51, 30]. Table 4 provides the details of these datasets and *azure*. Note the binning extent was selected in order to cover from roughly the 1% to the 99% percentiles of normalized values in the training data for each series (normalized using min-max scaling on the *conditioning* range; the prediction range can go below the min and above the max).

C.3 Metrics

Let i index the time series, and t index the time step. Let N be the total number of points $z_{i,t}$ on which we evaluate. Let $\mathcal{I}(\cdot)$ denote the indicator function. Let $\hat{z}_{i,t}^{(q\#)}$ be the $q\#$ quantile of the forecast distribution for time series i at point t , e.g. $\hat{z}_{i,t}^{(q\#.8)}$ is the value such that 80% of possible values for point $z_{i,t}$ are expected to be below this value.

We define *pinball loss* and *quantile loss* as part of the derivation of *weighted quantile loss*. *Weighted quantile loss*, *normalized deviation*, *calibration*, and *sharpness* are reported in the main paper.

Pinball loss:

$$\Lambda_\alpha(q, z) = (\alpha - \mathcal{I}(z < q))(z - q)$$

Quantile loss:

$$\text{QL}\# = \frac{\sum_{i,t} 2\Lambda_{(q\#)}(\hat{z}_{i,t}^{(q\#)}, z_{i,t})}{\sum_{i,t} |z_{i,t}|}$$

Weighted quantile loss:

$$\text{wQL} = \frac{1}{9}(\text{QL0.1} + \text{QL0.2} + \dots + \text{QL0.9})$$

Normalized deviation:

$$\text{ND} = \frac{\sum_{i,t} |z_{i,t} - \hat{z}_{i,t}|}{\sum_{i,t} |z_{i,t}|}$$

Calibration:

$$\text{calibration} = \frac{\sum_{i,t} \mathcal{I}(\hat{z}_{i,t}^{(q_l)} < z_{i,t} \leq \hat{z}_{i,t}^{(q_u)})}{N}$$

Sharpness:

$$\text{sharpness} = \frac{\sum_{i,t} |\hat{z}_{i,t}^{(q_u)} - \hat{z}_{i,t}^{(q_l)}|}{\sum_{i,t} |z_{i,t}|}$$

Where calibration and sharpness are reported together as the CovX metric. E.g., Cov80 gives the coverage and sharpness of the 80% prediction range where $q_l = q_{0.1}$ and $q_u = q_{0.9}$. Note that for all metrics we use 500 Monte Carlo samples in order to generate our forecast distribution, except for generating the Cov99 metrics in Table 1 of the main paper, for which we used 5000 samples, as the extreme percentiles are by definition more rare and require more samples for good estimation.

C.4 Background and motivation for our experimental setup

As mentioned in the main paper, multi-level C2FAR models actually include shallower models as special cases (i.e., a three-level C2FAR model is equivalent to a one-level model with a single bin in both the second and the third levels). So given enough tuning, C2FAR is strictly more powerful than a flat binning. Moreover, any shallower model (including a flat binning) could potentially be improved by adding additional finer-grained C2FAR levels, increasing the precision without making the problem any more complex for the original shallower model. We initially used this approach, adding a second C2FAR level to our production flat binning system and finding gains across all our internal and publicly-available datasets. In essence, the finer-grained C2FAR level acts as a kind of “reconstruction function” [51] for the coarse, flat binning model; the lower-level network maps the top-level bin to a more precise location. Adding another lower-level model increases the precision further, again, without any cost to the coarser predictions, and further levels can be added recursively until the optimum level of precision is obtained for the task at hand.

However, adding additional levels does have two practical costs: each level increases both the number of parameters (via the added networks at each level) and the number of hyperparameters (that is, the number of bins at each new level). Based on both theory and initial experimental results, we are therefore confident that we can pay this cost in order to achieve superior forecasting accuracy. However, for the purposes of this paper, we elected to pursue a different experimental question: for a fixed parameter budget (counting parameters across all levels in the C2FAR hierarchy), can we jointly tune the number of bins at each level in order to achieve superior predictions compared to traditional approaches? And can we do this without any additional cost for hyperparameter tuning? To answer this question, we established a fixed parameter budget of one million parameters for each system, and a budget of 100 tuning trials for each system.

C.5 Tuned and fixed hyperparameters

The specific parameters that are tuned are given in Table 5. Given tuning search space grows exponentially with added hyperparameters, we elected to fix some hyperparameters to values that proved effective in preliminary experiments (e.g., *lstm_dropout* and *n_lstm_layers*); other hyperparameters are either set to follow prior work (e.g., the conditioning range parameters), or are set for practical reasons in order to help maximize the use of our available compute resources. See Table 6 for a list of all fixed hyperparameters.

Recall that for forecasting, we tune for multi-step-ahead normalized deviation (ND) on the validation set. Whether tuning C2FAR models or tuning DeepAR-Gaussian, this requires running the Monte

Table 5: Tuning ranges for hyperparameter optimization.

Hyperparameter	Range	Sampling type
n_hidden	[16, 288]	integer
learning_rate	[1e-5, 1e-1]	loguniform
weight_decay	[1e-7, 1e-2]	loguniform
n_bins, for C2FAR-RNN ₁	[4, 1024]	integer
n_bins_level_ <i>i</i> , <i>i</i> th level of C2FAR-RNN _{<i>B</i>} , <i>B</i> > 1	[4, 128]	integer

Table 6: Fixed hyperparameters used in the empirical study.

Hyperparameter	Value	Note
n_max_total_parms	1,000,000	Enforced via a cap on n_hidden
lstm_dropout	1e-3	Intra-layer dropout
n_lstm_layers	2	
n_conditioning_range-hourly	168	For <i>elec</i> , <i>traff</i> , <i>azure</i> , as in prior work
n_conditioning_range-daily	30	For <i>wiki</i> , as in prior work
n_rollouts (validation)	25	For computing ND on validation set
n_rollouts (test)	500	For evaluation on test set
n_train_batch_size	1024	Total num. prediction ranges per batch
n_train_ranges_per_checkpoint	32768	Total num. prediction ranges in one <i>checkpoint</i> (train loss reported)
n_validation_set	32768	Total num. prediction ranges per validation evaluation
n_max_checkpoints	750	Maximum num. checkpoints (sets of n_train_ranges_per_checkpoint)
n_validation_eval_period	2	Num. train checkpoints per validation evaluation
n_validation_eval_warmup	11	Num. train checkpoints before first validation evaluation
n_stop_evals_no_improve	37	Num. validation evaluations without improvement before stopping

Carlo sampling procedure to generate a forecast distribution; we use the median of this forecast distribution as the point forecast for evaluation. Since sampling is relatively expensive, we evaluate only every second checkpoint, only after 11 warm-up checkpoints, on only 32768 validation prediction ranges, and only using 25 rollouts to generate the forecast distribution (note corresponding hyperparameters in Table 6). We also use smaller batch sizes for generating forecasts (testing) than we do in training (since we simultaneously vectorize over Monte Carlo rollouts for each series).

C.6 Tuning results

Table 7 provides the results of our tuning procedure in terms of the selected number of hidden units and bins. While prior work used a fixed 1024 bins in their flat binning [51], our tuner often selected quite fewer bins for C2FAR-RNN₁ on our datasets. C2FAR-RNN₂ and C2FAR-RNN₃

Table 7: Tuning results, tuning for normalized deviation, in the empirical study.

Dataset	System	nhidden	NBins1	NBins2	NBins3	Total bins	Total intervals
<i>elec</i>	DeepAR-Gaussian	141	-	-	-	-	-
<i>elec</i>	C2FAR-RNN ₁	248	110	-	-	110	110
<i>elec</i>	C2FAR-RNN ₂	189	12	35	-	47	420
<i>elec</i>	C2FAR-RNN ₃	156	5	25	21	51	2625
<i>traff</i>	DeepAR-Gaussian	165	-	-	-	-	-
<i>traff</i>	C2FAR-RNN ₁	236	163	-	-	163	163
<i>traff</i>	C2FAR-RNN ₂	184	28	13	-	41	364
<i>traff</i>	C2FAR-RNN ₃	146	17	9	5	31	765
<i>wiki</i>	DeepAR-Gaussian	153	-	-	-	-	-
<i>wiki</i>	C2FAR-RNN ₁	146	968	-	-	968	968
<i>wiki</i>	C2FAR-RNN ₂	176	21	18	-	39	378
<i>wiki</i>	C2FAR-RNN ₃	139	79	16	11	106	13904
<i>azure</i>	DeepAR-Gaussian	249	-	-	-	-	-
<i>azure</i>	C2FAR-RNN ₁	83	75	-	-	75	75
<i>azure</i>	C2FAR-RNN ₂	64	16	71	-	87	1136
<i>azure</i>	C2FAR-RNN ₃	130	16	11	94	121	16544

Table 8: Training time in hours for top system on validation set in empirical study.

	<i>elec</i>	<i>traff</i>	<i>wiki</i>	<i>azure</i>	Average
DeepAR-Gaussian	18.2	31.3	1.0	5.0	13.9
C2FAR-RNN ₁	28.7	27.1	12.8	12.8	20.3
C2FAR-RNN ₂	70.0	72.1	22.5	6.8	42.9
C2FAR-RNN ₃	29.5	57.1	32.3	31.5	37.6

Table 9: Time per 100 forecasts in *seconds* (running on NVIDIA Tesla P100) by top system on test set. All systems ran with common test batch sizes (60 for daily *wiki* dataset, 22 for hourly datasets) and number of samples (500) for each dataset.

	<i>elec</i>	<i>traff</i>	<i>wiki</i>	<i>azure</i>	Average
DeepAR-Gaussian	1.28	1.57	0.55	2.72	1.53
C2FAR-RNN ₁	3.73	3.79	1.71	1.34	2.64
C2FAR-RNN ₂	4.22	4.12	1.50	1.68	2.88
C2FAR-RNN ₃	4.81	4.45	1.92	4.73	3.98

models generally use fewer total bins than flat binning, while having very many more total actual intervals.

C.7 Computational performance and resource requirements

Table 8 has the training times for the top systems found on the validation set. Training time naturally reflects both the speed of convergence in learning (number of training epochs) *and* the speed of operating the specific architecture.⁶

Testing time roughly follows a similar pattern (Table 9), taking longer on the multi-level C2FAR models, although more efficient implementations than ours are certainly possible. Meanwhile, Table 10 gives the memory requirements of the different systems. Overall, we may say that in our implementation, multi-level C2FAR models run slower than a flat binning, but with less memory.

C.8 Evaluation by forecast horizon

Figure 14 shows the forecast error of the systems as a function of the forecast horizon. Compared to three baselines (Naïve, Seasonal-naïve and DeepAR-Gaussian), we find C2FAR-RNN₃ is the best performer across virtually all horizons on all datasets, except the last couple horizons on *azure*. Interestingly, before C2FAR, practitioners faced a very nuanced problem when selecting a forecast method for their own dataset. E.g., on the cloud demand data that we are most interested in (*azure*), and ignoring C2FAR, it seems that on some horizons, Naïve is best, on others, DeepAR, and on others still, it is Seasonal-naïve. C2FAR combines the best aspects of all of these systems, outputting highly-

⁶Note that the baseline systems Naïve, Seasonal-naïve, and ETS do not require training; ETS parameters are fit separately for each input history at *inference* time.

Table 10: Amount of memory consumed for prediction in MiB (measured via *nvidia-smi* on NVIDIA Tesla P100) by top system on test set. All systems ran with common *test batch sizes* (60 for daily *wiki*, 22 for hourly datasets) and number of samples (500) for each dataset. The flat binning, C2FAR-RNN₁, consumes significantly more memory on three of the four datasets; memory requirements depend directly on the number of bins selected by the tuner (see Table 7).

	<i>elec</i>	<i>traff</i>	<i>wiki</i>	<i>azure</i>	Average
DeepAR-Gaussian	4295	4873	3113	4845	4281.50
C2FAR-RNN ₁	8264	7465	12619	3389	7934.25
C2FAR-RNN ₂	6233	6147	5577	4209	5541.50
C2FAR-RNN ₃	5657	5111	6372	6037	5794.25

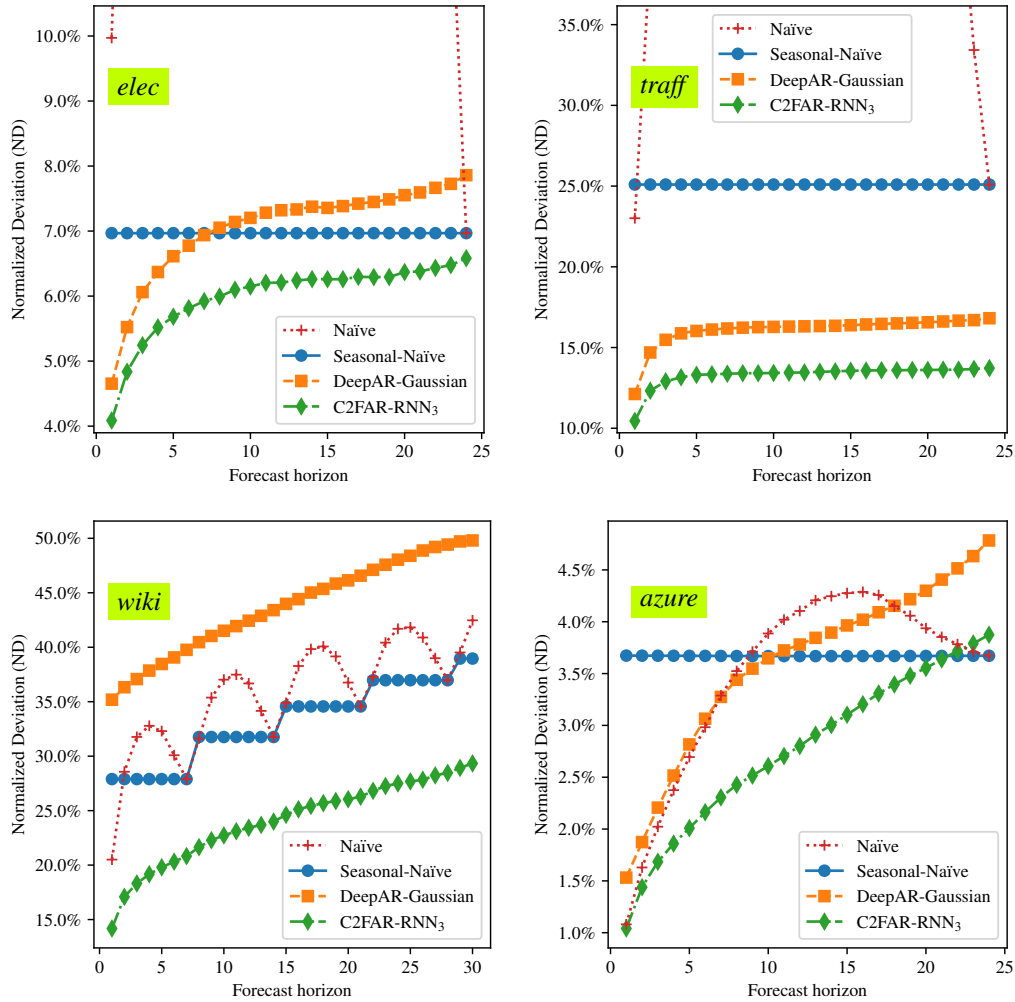


Figure 14: Comparison of different forecasting systems with normalized deviation (ND) calculated separately at each forecast horizon. For *elec*, *traff*, and *azure*, we forecast forward for one 24-hour seasonal cycle, while for *wiki*, we predict for slightly-more-than-four 7-day cycles. Seasonal-naïve is flat over a cycle because we evaluate using rolling predictions: every datapoint is forecast once at every horizon, and always gets the same prediction. Vanilla Naïve becomes first less accurate, then more accurate as we approach the end of the cycle, at which point it becomes equivalent to Seasonal-naïve. Aside from *wiki*, where DeepAR-Gaussian fails to learn a good model, DeepAR-Gaussian is competitive with C2FAR-RNN₃ at earlier horizons, but the gap widens over time.

precise predictions when doing so makes sense (similar to Naïve), but generating seasonally-adjusted estimates during the middle forecast horizons.

D Stability of Empirical Results

In this section, we investigate the stability of our empirical results. Random seeds are used in both our testing process (via Monte Carlo sampling of predicted future values) and our tuning process (via sampling of hyperparameters), and it is important to quantify the stability of these sources of randomness separately [16]. Ideally, we would repeat our entire tuning procedure multiple times with different random seeds, allowing us to determine the reliability of our process for fitting both model parameters and hyperparameters. While such repetition is not practical given the total time required, we can nevertheless investigate tuning randomness in other ways, and use this to assess the stability of our empirical results. Note that stability of results may depend on both the systems under investigation (e.g., models with more hyperparameters may be more unstable with respect to tuning), the datasets and splits used in the experiments (e.g., larger data sets may be more stable), and the tuning/training/testing processes (e.g., more tuning runs may lead to more stable results).

We summarize the results as follows, but provide full details in the following subsections:

- The Monte Carlo sampling process is very stable with respect to the random seed: we repeated the sampling 6 times and found negligible differences in normalized deviation (§D.1).
- Results are fairly stable when moving from the validation set to the test set: on all validation sets and all test sets, the top C2FAR models improve on the top DeepAR-Gaussian model. On all validation sets and all test sets, C2FAR-RNN₂ performed better than C2FAR-RNN₁. However, in testing three of the four datasets, C2FAR-RNN₃ improved over its ranking on the validation set (§D.2).
- Results are less stable with respect to the tuning. If we use the second-best validation-set model on each *test* set, C2FAR-RNN₃ and C2FAR-RNN₂ suffer larger drops on test than C2FAR-RNN₁, while DeepAR-Gaussian improves in two cases. However, even with the second-best models, C2FAR models perform better than DeepAR-Gaussian across all test sets, and C2FAR-RNN₃ remains the top system on three of the four test sets (§D.3).

Note we do not assess the stability of re-training the models with the same hyperparameters, but different shuffling of the training data, as such re-training is not currently part of our operations. However, as future work, we plan to investigate the stability of re-training-without-re-tuning in the context of slight increases in the training data over time, which is very common in real-world ML pipelines.

D.1 Sampling stability

Recall that prediction of each example creates a forecast distribution using 500 different Monte Carlo rollouts of the time series. We take the median of this distribution to compute the normalized deviation (ND). Overall ND is the average over all test examples, and we report this in Table 1 of the main paper. We repeated the ND evaluation of our models 6 times using different random seeds, and plotted the distribution of the 6 results as *violin plots* in Figures 15 to 18. The distributions are very narrow, showing that average ND is very stable with respect to the random seed. We conclude that evaluation is very stable with respect to the random seed used in Monte Carlo sampling.

D.2 Validation/test stability

Another possible source of instability is different behavior of systems on the validation set versus the test set. We summarize this behavior in our data by showing the ranking of the systems on the validation set and test set in Table 11 (note we exclude DeepAR-Gaussian from this table as it is always ranked 4th on all validation and test sets). Results are fairly stable moving from validation to test. On all validation sets and all test sets, all C2FAR models improve over DeepAR-Gaussian. Also, on all validation sets and all test sets, C2FAR-RNN₂ improves over C2FAR-RNN₁. The ranking in *traff* is the same on validation and test set, but on the others, the only difference is C2FAR-RNN₃ moved to first place on test.

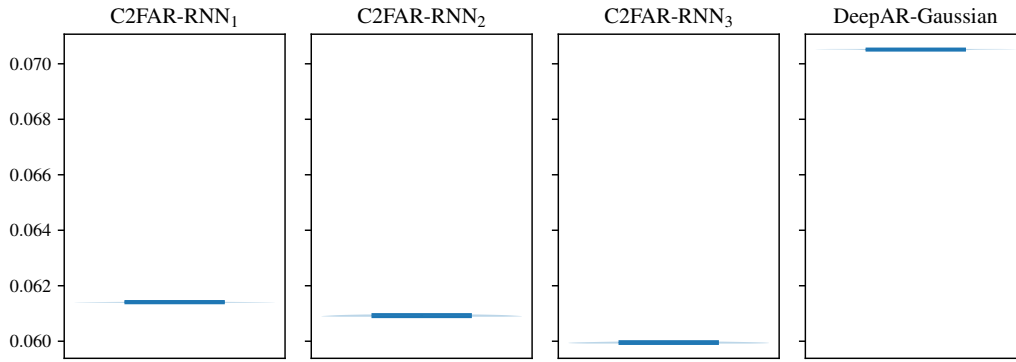


Figure 15: *elec* sampling stability: distribution of normalized deviation (on test set) across different random seeds as a violin plot.

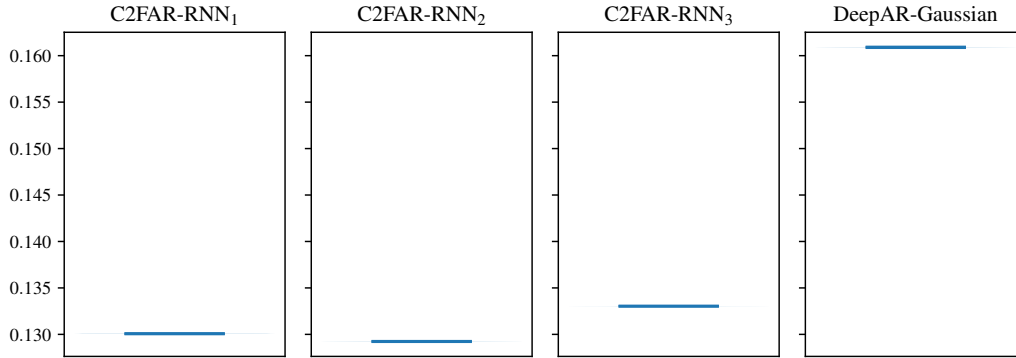


Figure 16: *traff* sampling stability: distribution of normalized deviation (on test set) across different random seeds as a violin plot.

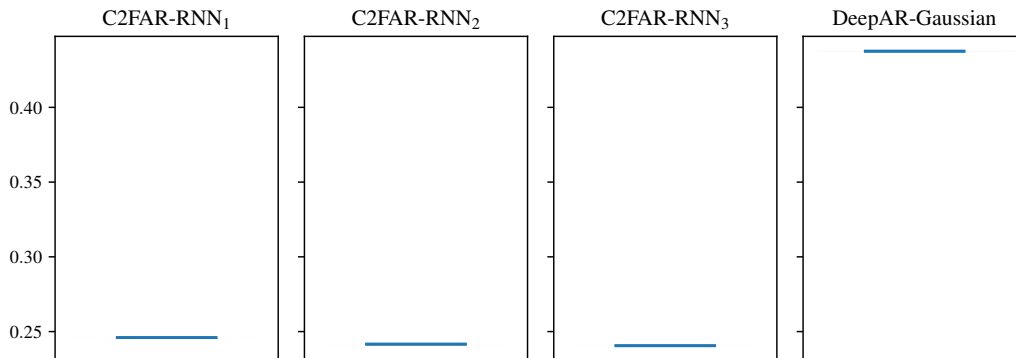


Figure 17: *wiki* sampling stability: distribution of normalized deviation (on test set) across different random seeds as a violin plot.

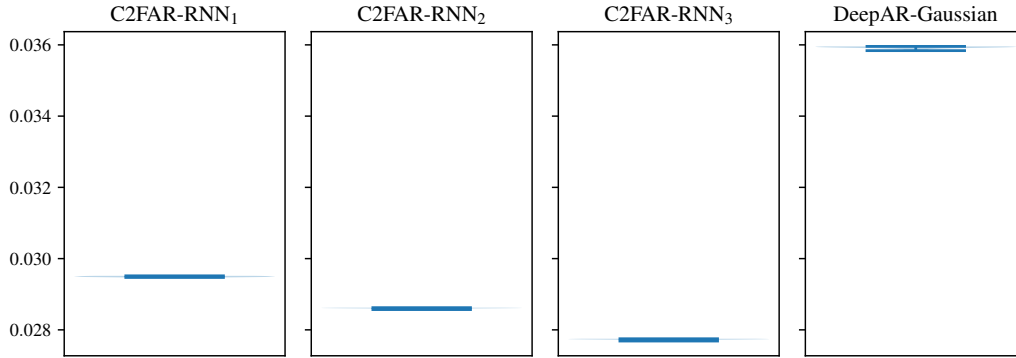


Figure 18: *azure* sampling stability: distribution of normalized deviation (on test set) across different random seeds as a violin plot.

Table 11: Validation/test stability

	1st	<i>elec</i> 2nd	3rd	1st	<i>traff</i> 2nd	3rd
Val.	C2FAR-RNN ₂	C2FAR-RNN₃	C2FAR-RNN ₁	C2FAR-RNN ₂	C2FAR-RNN ₁	C2FAR-RNN ₃
Test	C2FAR-RNN₃	C2FAR-RNN ₂	C2FAR-RNN ₁	C2FAR-RNN ₂	C2FAR-RNN ₁	C2FAR-RNN ₃
	1st	<i>wiki</i> 2nd	3rd	1st	<i>azure</i> 2nd	3rd
Val.	C2FAR-RNN ₂	C2FAR-RNN ₁	C2FAR-RNN₃	C2FAR-RNN ₂	C2FAR-RNN₃	C2FAR-RNN ₁
Test	C2FAR-RNN₃	C2FAR-RNN ₂	C2FAR-RNN ₁	C2FAR-RNN₃	C2FAR-RNN ₂	C2FAR-RNN ₁

D.3 Tuning stability

We assess the stability of our tuning results by considering the consequences had the optimizer not found the top model on the validation set. We therefore evaluate the second-best models from the validation set on the test set. We hypothesize that the second-best models may have larger drops for C2FAR-RNN₂ and C2FAR-RNN₃, as these models have more hyperparameters and are therefore more vulnerable to sub-optimal tuning. Figures 19 to 22 show the results, with the blue lines indicating the original top-model result, and the red lines indicating the result after switching to the second-best validation model.

We do see larger drops for the multi-level C2FAR models, especially C2FAR-RNN₂, which drops significantly on the *elec* dataset. However, even with the second-best models, C2FAR models perform

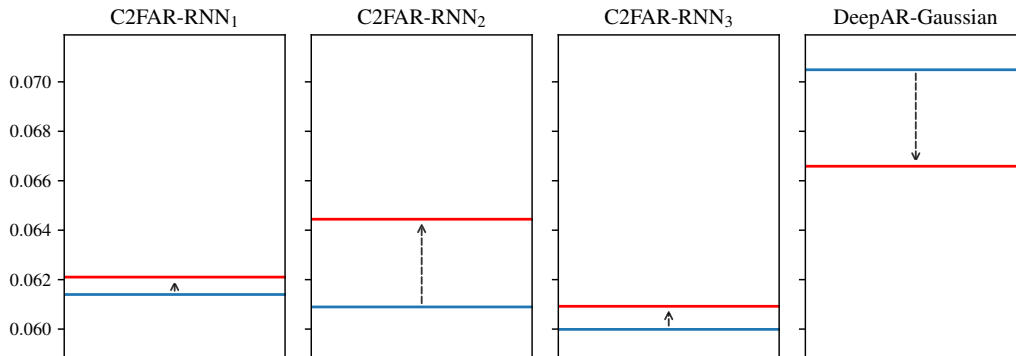


Figure 19: *elec* tuning stability: difference in normalized deviation (on test set) from top-1 tuned model (in blue) to second-best tuned model (in red).

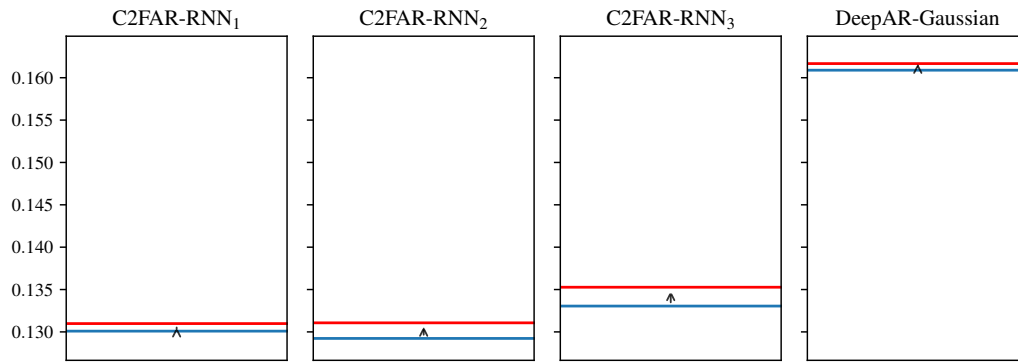


Figure 20: *traff* tuning stability: difference in normalized deviation (on test set) from top-1 tuned model (in blue) to second-best tuned model (in red).

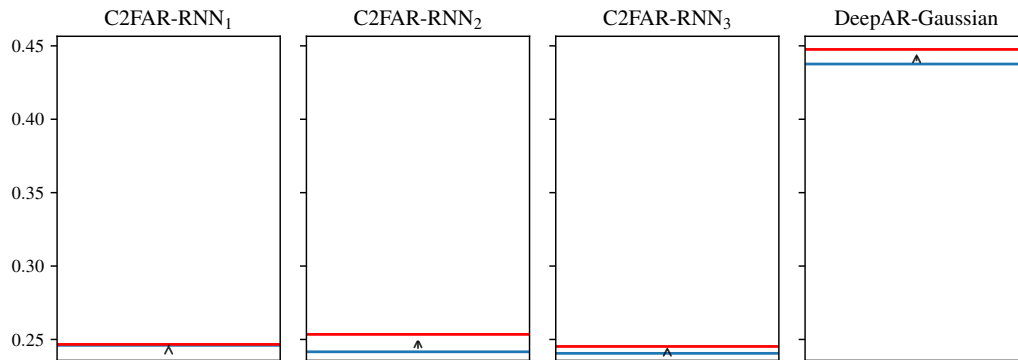


Figure 21: *wiki* tuning stability: difference in normalized deviation (on test set) from top-1 tuned model (in blue) to second-best tuned model (in red).

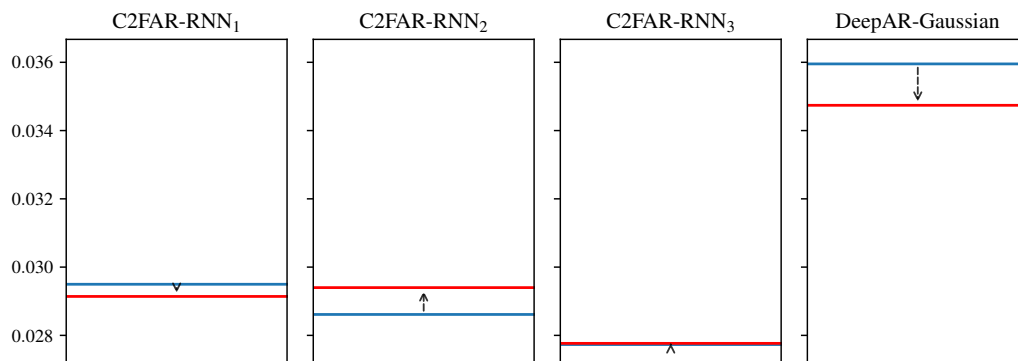


Figure 22: *azure* tuning stability: difference in normalized deviation (on test set) from top-1 tuned model (in blue) to second-best tuned model (in red).

Table 12: Tuning results, tuning for NLL, on *azure* with noise added. Compare to Table 7 for tuning for ND.

Dataset	System	nhidden	NBins1	NBins2	NBins3	Total bins	Total intervals
<i>azure</i>	DeepAR-Gaussian	74	-	-	-	-	-
<i>azure</i>	C2FAR-RNN ₁	165	638	-	-	638	638
<i>azure</i>	C2FAR-RNN ₂	126	70	31	-	101	2170
<i>azure</i>	C2FAR-RNN ₃	141	6	14	67	87	5628

Table 13: NLL results on noisy and original datasets

Dataset	Trained for	Experimental configuration				System			
		Tested for	Tuned for	Trained on	Tested on	DeepAR-Gaussian	C2FAR-RNN ₁	C2FAR-RNN ₂	C2FAR-RNN ₃
<i>azure</i>	NLL	NLL	NLL	+Noise	+Noise	1.355	-2.011	-2.075	-2.075
<i>azure</i>	NLL	NLL	ND	Original	+Noise	0.766	-1.739	-1.574	-1.504
<i>azure</i>	NLL	NLL	NLL	+Noise	Original	2.307	-3.300	-4.110	-4.043
<i>azure</i>	NLL	NLL	ND	Original	Original	0.094	-2.533	-4.475	-6.309

better than DeepAR-Gaussian across all test sets, and C2FAR-RNN₃ remains, as before, the top system on three of the four test sets (§D.3). Overall, this suggests that we may wish to use more tuning trials for the multi-level C2FAR models, or, as suggested in the main paper, simply use the same number of bins at each level, reducing the number of bins to a single hyperparameter, as in the flat binning.

E Test-set likelihood experiments

In this section, we report some supplementary results comparing our systems for their ability to estimate the log-likelihood of held-out test data. As mentioned in the main paper in §4.2, log-likelihood is sometimes regarded as the de facto standard for evaluating generative models [69], and results on log-likelihood estimation are regarded as a proxy for the effectiveness of models on other tasks such as anomaly detection or missing value imputation. Since we cannot *tune* C2FAR models directly for log-likelihood on discrete data (as this leads to narrower and narrower density spikes), we investigate models trained under two other regimes:

1. Models tuned for ND (that is, the same models used in the forecasting experiments)
2. Models tuned for negative log likelihood (NLL), but on *dequantized* data, i.e., data with `Uniform[0, 1]` noise added, as in prior work [54]

For the models tuned for NLL on the noise-added data, we use the same tuning setup as in forecasting, doing 100 tuning evaluations for each system and using the same tuned and fixed hyperparameters as described in §C.5. We performed this experiment on *azure* data only.

The resulting tuned hyperparameters are given in Table 12. Interestingly, the tuner selects quite many more bins for the C2FAR-RNN₁ model as were selected when tuning for ND (Table 7), suggesting precision is important even in noise-added data.

We evaluated both the NLL- and ND-tuned systems on both the original test data and the test data with `Uniform[0, 1]` noise added. Results are given in Table 13. Likelihood is computed in the normalized domain (after min-max scaling) for all time series.

We can divide the evaluation into two objectives: NLL on the noise-added data, and NLL on the original data. If our objective is NLL on the noise-added data, then we see that multi-level C2FAR models still offer benefits over a flat binning. One may have expected this to not be the case, as adding noise removes some of the precision in the data and thus one of the advantages of C2FAR, but we see that both C2FAR-RNN₂ and C2FAR-RNN₃ still prove superior to the flat binning in this case. Even on noise-added data, multi-level C2FAR models use many more total intervals than those used by a flat binning (Table 12), illustrating that precision is still important even in noise-added data.

Now, regarding NLL of the *original* data, we see that multi-level C2FAR models are again superior to flat binning, and moreover, multi-level C2FAR models trained for ND are superior to those trained for NLL on the noise-added data. This illustrates that, if our objective is to achieve maximum likelihood on the original data, adding noise to dequantize the data may not be a good solution; here it results in worse NLL than simply tuning for ND on the original data. We repeat the point in the main paper that, in reality, for tasks such as anomaly detection, missing value imputation, denoising, compression, etc., we should not tune for NLL at all, but rather tune for the application-specific metric of interest.